Groundbased Instrumentation for Measurements of Atmospheric Airglow

A Thesis
Submitted to the College of Graduate Studies and Research
in Partial Fulfillment of the Requirements
for the Degree of
Master of Science
in the
Department of Electrical Engineering
University of Saskatchewan

by
Paul Robert Parker Loewen
Saskatoon, Saskatchewan

In presenting this thesis in partial fulfillment of the requirements for a Postgraduate degree from the University of Saskatchewan, the author agrees that the Libraries of this University may make it freely available for inspection. The author further agrees that permission for copying of this thesis in any manner, in whole or in part, for scholarly purposes may be granted by the professor who supervised this thesis work or, in his absence, by the Head of the Department or the Dean of the College in which this thesis work was done. It is understood that any copying or publication or use of this thesis or parts thereof for financial gain shall not be allowed without written approval from the author. It is also understood that due recognition shall be given to the author and to the University of Saskatchewan in any scholarly use which may be made of any material in this thesis.

Requests for permission to copy or to make other use of material in this thesis in whole or in part should be addressed to:

Head of the Department of Electrical Engineering
University of Saskatchewan
Saskatoon, Saskatchewan
Canada S7N 5A9

To my family: Deb, Rob, Sarah and Trent

Abstract

A groundbased instrument to measure the atmospheric airglow of the molecular oxygen infrared atmospheric band emission was designed, built, tested and operated. The two channel photometer constructed was based on the original design by Evans (1967) that had been used in balloon experiments.

The two channel photometer system specifications are presented. The major difference between the presented design and the earlier two channel photometers is the detector. An Indium Gallium Arsenide (InGaAs) photodiode provided better signal to noise in the conversion of the infrared light signal to an electronic signal than the previously used Lead Sulphide (PbS) detectors.

The completed instrument was tested to determine its performance characteristics. Through these tests it was found that the photometer output offset is sensitive to ambient temperature fluctuations. An analysis of the instrument noise was done in an attempt to explain this sensitivity. The output noise performance was characterized and is presented together with the absolute brightness and wavelength calibrations.

Data was collected with the instrument in Saskatoon, SK and Eureka, NU. After an initial observation campaign in the high arctic (Eureka, NU) modifications were made to the environmental housing of the instrument in order to improve the scientific value of the data collected. The collected data was processed and a simple analysis performed to demonstrate the capability of the photometer to measure the infrared atmospheric airglow.

The collected data can be used to determine the mesospheric ozone height profile. The required data analysis to do so is beyond the scope of this presentation. However, the presented data does demonstrate that the designed and constructed two channel photometer can make the necessary measurements.

Acknowledgements

First I would like to thank Brian Howe and the Meteorological Service of Canada for providing me with the opportunity to visit the high Arctic which was one of my goals when starting the project.

I would also like to thank Dave Karaloff and Vic Meyer for their time and effort in providing help with electronic parts and producing my printed circuit boards. A big thank you to Dr. Nick Lloyd whose experience and knowledge was always appreciated. For their help when I was stuck and for keeping my time throughout the project entertaining I would like to thank my office partners Adam Bourassa and Truitt Wiensz. An additional thanks to Adam for letting me know about this opportunity and his constant support and encouragement throughout.

Finally I would like to express my appreciation for my supervisors. Dr. S.O. Kasap, for giving me this opportunity and always making time to provide assistance. Dr. Ted Llewellyn, his practical knowledge in building and operating a two channel photometer was always invaluable information. I would also like to thank Ted for his enthusiasm and dedication to making a strong team orientated working environment. Dr. Doug Degenstein, for his time and effort in helping me throughout the project. Doug always managed to explain concepts in an understandable way and guided me in the right direction when I needed it. To all three I would just like to say thank you again, I learned a lot and had fun doing it.

Contents

List of Figures

List of Tables

Glossary of Terms

A	Einstein Coefficient.
AC	Alternating Current.
B	Brightness $[photons/cm^2/s/nm/ster]$.
DC	Direct Current.
DN	Digital Number. Units of data output from TOP2000.
EHPs	Electron hole pairs.
h	Planck's constant.
InGaAs	Indium Gallium Arsenide.
IRIS	InfraRed Imaging System; specifically the three linear array imagers of the OSIRIS instrument.
ISAS	Institute of Space and Atmospheric Studies
k	Absolute Calibration Constant.
λ	Total decay time constant.
LIA	Lock-in amplifier.
PID	Proportional Integral Derivative.

TOP2000	The two channel photometer designed and developed for this thesis project.
ν	Frequency.
Odin	A Swedish led remote sensing satellite launched on February 20, 2001.
OSIRIS	Optical Spectrograph and InfraRed Imaging System. A Canadian built remote sensing instrument on board the satellite Odin.
QE	Quantum Efficiency.
SME	Solar Mesospheric Explorer.
T	Temperature.
UV	Ultraviolet.
V	Volume emission rate $[photons/cm^3/s/nm/ster]$.

Chapter 1

Introduction

1.1 Atmospheric Airglow Measurements

The study of atomic and molecular emissions in the atmosphere, referred to as the airglow, provides information on chemical and physical processes in the atmosphere. Over the years several techniques have been developed to measure these emissions on different platforms such as groundbased, balloons, rockets and satellites. As the technology improves, and cost is reduced, satellite missions are becoming more popular for airglow measurements. Satellite data can provide uninterrupted global coverage in a relatively short time and continued monitoring over a period of years. While groundbased instruments cannot provide the same global coverage they can be used to monitor the airglow at a specific location for an extended period. Groundbased measurements also provide verification of the satellite data.

1.2 Statement of Objectives

The main objective of this project was to design and build an instrument that could reliably measure the emission from the excited state of molecular oxygen in the atmosphere. The new design was based on the previously built two channel

photometers that had been used to measure the height profile of the oxygen airglow. The improvements over the previous design included updating the detector to take advantage of the reduced noise equivalent power (NEP) that is provided by indium gallium arsenide (InGaAs) detectors compared to the originally used lead sulphide (PbS) detectors and to minimize user intervention during data collection by the instrument. The instrument also had to operate in the harsh environment of the high arctic.

1.3 The OSIRIS Imager

The optical spectrograph and infrared imager system (OSIRIS) is the Canadian contribution to Odin, a Swedish-led remote sensing satellite. The optical spectrograph (OS) measures atmospheric emissions and absorptions in the UV-visible regions. The infrared imager system (IRIS) consists of three separate imagers with the first two focused on measurements of the molecular oxygen infrared atmospheric band emission ($a^1\Delta_g - X^3\Sigma_g^-$), see Appendix A for information on the spectral transitions. Measurements of this band are relevant to the study of mesospheric ozone and a few other species that are important in the chemistry and dynamics of the atmosphere.

1.4 Groundbased Airglow Measurements

Even though groundbased instruments do not offer the global coverage of satellites they can provide accurate local data at low cost. A current version of the groundbased instrument, which is based on earlier designs, was developed to measure the same emission band as the infrared imager system OSIRIS. These measurements can provide a calibration verification for OSIRIS. The groundbased instrument also permits experiments to determine the twilight decay rates and emission band brightness altitude profiles to be made. If these measurements are made over an extended period of time at a given location they can be used to observe trends in the atmo-

sphere that are related to those processes involved in the production of the singlet delta emission.

1.5 Summary of Presentation

A history of the infrared atmospheric band emission measurements is given in Chapter 2. The relevant chemistry for the infrared atmospheric band emission is presented together with the two channel photometer technique used to measure the brightness of the band emission. The ability of groundbased measurements from the two channel photometer to provide ozone concentration profiles and singlet delta emission decay rates is also demonstrated.

An overall description of the two channel photometer setup and the design detail for each section of the instrument is given in Chapter 3. The wavelength and absolute brightness calibrations and the observed output characteristics of the constructed photometer are presented in Chapter 4. An analysis of the output offset and its temperature dependence and the noise performance of the photometer are also included in Chapter 4.

The experimental observations are presented in Chapter 5. The modifications to the instrument setup during data collection in Saskatoon, SK and Eureka, NU through 2003-2004 are outlined and the processed data is shown. The analyzed data and its application to determine the singlet delta decay rates to verify the scientific value of the constructed photometer is presented in Chapter 6. Finally a summary of the present work and recommendations for future work are given in Chapter 7.

Chapter 2

Background

2.1 Introduction

This chapter includes a brief history of singlet delta measurements from its original discovery in the atmosphere by Herzberg [1] to the current satellite measurements being made by the OSIRIS instrument. The photochemical processes involved in the production of singlet delta, specifically production from ozone photolysis, are discussed. The evolution of the two channel photometer and the measurement technique for singlet delta, the possibility of ozone retrievals from the photometer measurements and the decay rate at given atmospheric altitudes are also presented.

2.2 History of Singlet Delta Measurements

Using infrared sensitive plates Herzberg first measured the atmospheric infrared oxygen band between 12,500 Å and 12,750 Å when photographing the solar spectrum [1]. With the introduction of PbS infrared detectors Vallance Jones and Harrison attempted to observe the theorized 0,0 $O_2(a^1\Delta_g - X^3\Sigma_g^-)$ emission band at 1.27 μm [2], where 0,0 represents the vibrational state of the excited (singlet delta) and ground states of molecular oxygen respectively. The 1.27 μm emission was not

detected. However, they did measure the 0,1 $O_2(a^1\Delta_g - X^3\Sigma_g^-)$ emission band at 1.58 μm. The suggested reason for the unsuccessful detection of the 1.27 μm band emission was reabsorption by oxygen in the lower atmosphere. Using an airborne spectrometer Noxon and Vallance Jones [3] successfully measured the 0,0 band at 1.27 μm during the day and twilight.

The mechanisms responsible for excited atmospheric molecular oxygen (singlet delta) were originally believed to be resonant-phosphorescence and chemical reactions between atomic oxygen and ozone. Later measurements by Vallance Jones and Gattinger [4] showed a strong seasonal dependence and a much longer decay of the emission brightness than could be explained by the resonant-phosporescence theory. Vallance Jones and Gattinger proposed that singlet delta was produced by the photodissociation of ozone in the Hartley continuum. While the photodissociation model agreed with the observed data there was no explanation for the seasonal variations. Airborne observations of the 0,0 band conducted by Gattinger and Vallance Jones [5], Noxon [6] and Evans *et al.* [7] subsequently supported the ozone dissociation mechanism.

The first altitude profile of the 0,0 band at 1.27 μm was measured in the day using a two channel photometer flown in a rocket [8]. The observed profile agreed with that predicted for ozone dissociation except for an unexplained increase in emission just above 80 km. Later rocket measurements confirmed the excess emission [9], [10].

As mentioned the 0,0 band at 1.27 μm is strongly absorbed by molecular oxygen and so limited early ground measurements to the less intense 0,1 band at 1.58 μm, which is not absorbed. As technology improved measurements of the 0,0 band from the ground became possible. Lowe first reported ground based observations of the 0,0 band in the late evening using a Michelson interferometer [11]. These measurements and the atmospheric transmission calculations of Evans *et al.* predicted that between 4 and 6% of the 0,0 band emission intensity is transmitted to the ground [12]. Several ground based measurements of the 0,0 band were made using a modified version of

the two channel photometer that was orignally developed for rocket and balloon experiments [13]. A technique for inferring the altitude profiles of the 1.27 μm emission was developed and the derived altitude distributions compared with rocket measurements. This demonstrated that the ground based photometer technique is a practical method to monitor twilight altitude distributions of singlet delta [14]. The next several years saw intermittent two channel ground based measurement campaigns. These included ground and rocket measurements [10], evening twilight and solar eclipse measurements at Great Whale River, PQ [15] and high arctic observations in Alert, NU [16].

By the early 1980's satellites had become a popular technique for measuring and monitoring the atmosphere. The Solar Mesosphere Explorer (SME) spacecraft was launched in 1981 with the objective of studying ozone in the Earth's atmosphere. One instrument on the SME used to measure ozone density was the near-infrared spectrometer, this provided the first satellite measurements at 1.27 μm. The results of the satellite measurements confirmed that the excess emission peak above 80 km is largely due to ozone [17] and that the day-to-day and seasonal variations could be explained by temperature changes in the atmosphere that modulated the ozone concentration profile [18].

The improvement in measurement techniques and technology over the years has allowed for a better understanding of the atmospheric model, specifically ozone determination from measurements of singlet delta. Currently linear infrared imagers in the OSIRIS instrument on board the Odin satellite, launched February 2001, provide vertical limb measurements over an altitude range of approximately 100 km. The line of sight measurements are used with a tomographic inversion technique to provide altitude profiles of the 1.27 μm emission brightness for the global coverage of the satellite [19], [20].

2.3 Singlet Delta Photochemistry

The production of $O_2(a^1\Delta_g)$ (singlet delta) and its lifetime in the atmosphere depend on the solar input, atmospheric concentrations and chemical processes. The altitude distribution of various atmospheric species and the rising and setting of the sun makes the singlet delta emission brightness both altitude and time dependent.

The 0,0 band emission at 1.27 μm results from the transition of excited state molecular oxygen to the ground state as described in equation 2.1.

$$O_2(a^1\Delta_g) \rightarrow O_2(X^3\Sigma_g^-) + h\nu \tag{2.1}$$

where $O_2(X^3\Sigma_g^-)$ is the ground state of molecular oxygen and $h\nu$ is the energy of the emission at 1.27 μm.

The $O_2(a^1\Delta_g - X^3\Sigma_g^-)$ emission is not a single wavelength at 1.27μm but rather a spectrum determined by the rotational states of the molecule. The calculated line spectrum at 0°C for the $O_2(a^1\Delta_g - X^3\Sigma_g^-)$ transition is shown in Figure 2.1. In the atmosphere this spectrum is shaped by both temperature and pressure.

The major processes involved in the atmospheric production of singlet delta are shown in Figure 2.2 [21]. The primary production mechanism is due to ozone photodissociation by ultra violet sun light (J_H in Figure 2.2) in the Hartley band (210-310 nm) as described in equation 2.2.

$$O_3 + h\nu \rightarrow O_2(a^1\Delta_g) + O(^1D) \tag{2.2}$$

where $h\nu$ is the input solar radiation in the Hartley band and $O(^1D)$ is an excited state of atomic oxygen.

The chemical processes resulting from the production of $O(^1D)$ through photolysis of ground state molecular oxygen in the Schumann-Runge continuum (J_{src}, wavelengths less then 175 nm) and in the Lyman alpha (J_α) spectral regions (175-200 nm) are given in equations 2.3 and 2.4.

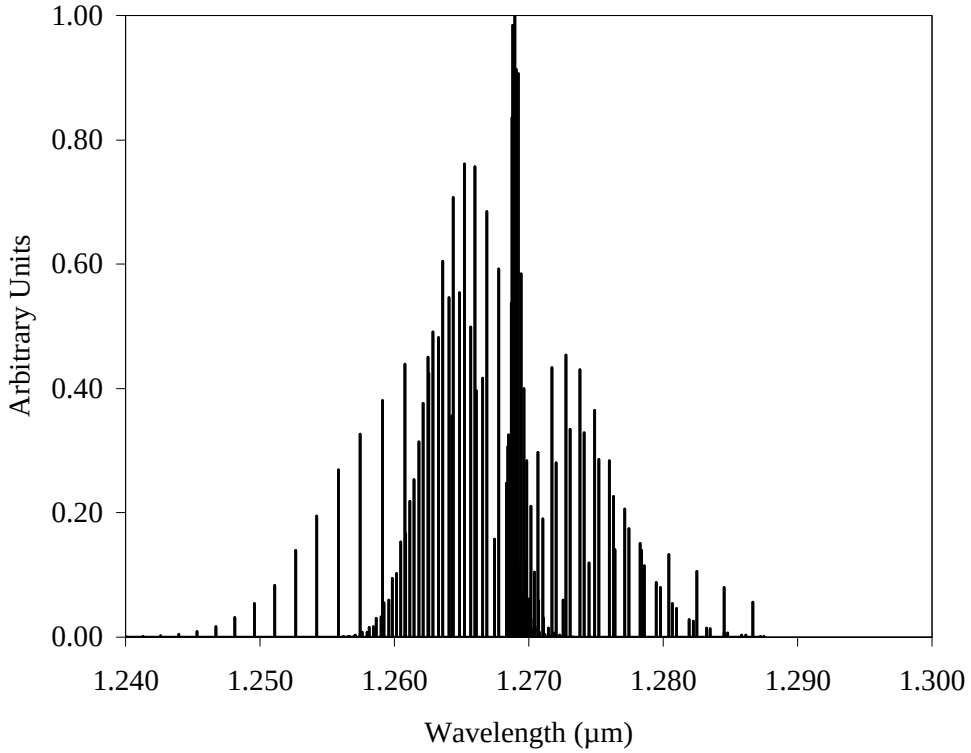

Figure 2.1: Line Spectrum of the 0,0 $O_2(a^1\Delta_g - X^3\Sigma_g^-)$ emission at 0°C.

$$O(^1D) + O_2 \rightarrow O_2(b^1\Sigma_g^+) + O(^3P) \tag{2.3}$$

$$O_2(b^1\Sigma_g^+) + Q \rightarrow O_2(a^1\Delta_g) + Q \tag{2.4}$$

where $O_2(b^1\Sigma_g^+)$ is another excited state of molecular oxygen, $O(^3P)$ is the ground state of atomic oxygen and Q is any atmospheric molecule. As well as the radiative transition of singlet delta to ground state there is also quenching as given by equation 2.5.

$$O_2(a^1\Delta_g) + Q \rightarrow O_2(X^3\Sigma_g^-) + Q \tag{2.5}$$

These processes, equations 2.1 through 2.5, are summarized in Figure 2.2.

It is apparent from the described chemical and physical processes that the intensity of the singlet delta emission at a given altitude will depend mainly on the amount of ozone and the ultra violet solar irradiance. The actual altitude dependence is also determined by the radiative and quenching lifetimes. The effective lifetime of the $O_2(a^1\Delta_g)$ molecule, between 30 and 100 kilometers, is given in Figure 2.3. The radiative lifetime (1/A), where A is the Einstein spontaneous coefficient (the probability that a molecule will radiate per second), is approximately 65 minutes. The quenching lifetime profiles in Figure 2.3 are based on the Mlynczak *et al.* model [21], which uses O_2, N_2 and O for the quenching species and the Sica model [22] which considers only O_2 quenching. It is apparent that only at high altitudes is the quenching by atomic oxygen a contributor to the quenching lifetime of singlet delta. Also by comparison with the Sica model quenching by N_2 is insignificant. At lower altitudes (30-70 km) the quenching process dominates and the total singlet delta lifetime is significantly less than the radiative lifetime. At about 75 km the quenching lifetime and radiative lifetime are equal. Above 75 km the radiative lifetime dominates as the probability of quenching is significantly reduced in the low density atmosphere.

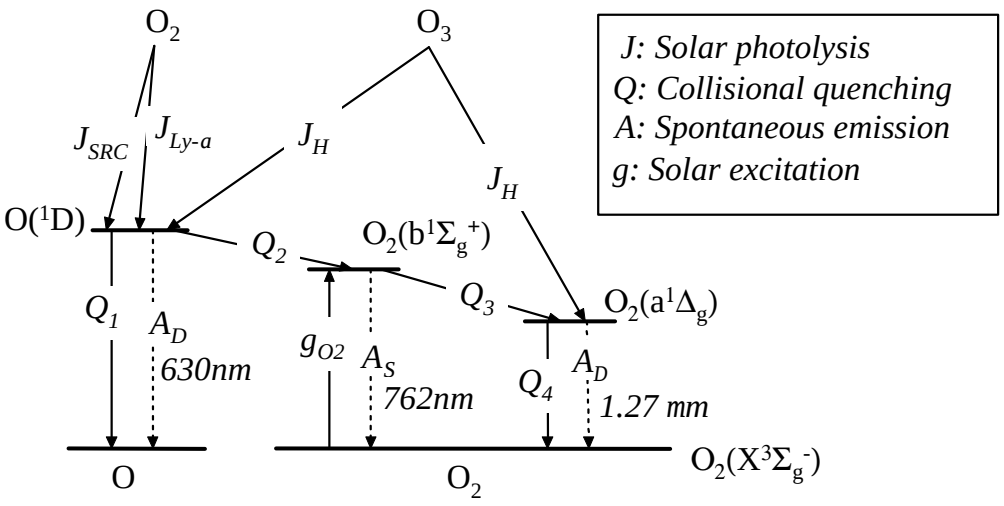

Figure 2.2: Illustration of processes resulting in 1.27μm emission [21].

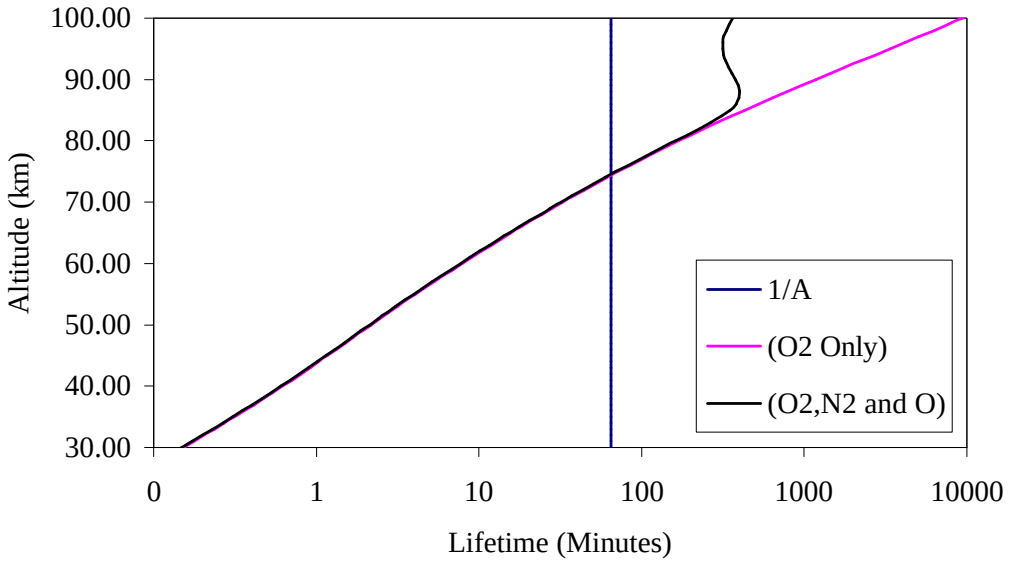

Figure 2.3: Radiative Lifetime (1/A) and Quenching Lifetimes from two models for singlet delta.

2.4 Groundbased Photometer Setup

The two channel photometer that was originally developed for balloon and rocket measurements of the 1.27 μm emission in the atmosphere is described by Evans [23]. This two channel photometer technique also proved to be an accurate method of detecting singlet delta from the ground.

From the ground the photometer looks straight up with a small field of view of 5° over which brightness is assumed to be uniform. The signal brightness (B $[photons/cm^2/s/nm/ster]$) measured at the ground is the integral of the volume emission rates (V $[photons/cm^3/s/nm/ster]$) in the vertical column line of sight, equation 2.6.

$$B = \int_0^\infty V(h)\alpha(h)dh \tag{2.6}$$

where h is the height and α is the attenuation of the volume emission from the given altitude to the ground.

During the day and early twilight the brightness (B) at the ground is due to both scattered sunlight and the singlet delta emission at 1.27 μm. As the sun sets two shadow heights are formed, this is illustrated in Figure 2.4. The ultra violet light responsible for ozone photolysis and the generation of singlet delta is attenuated as the sun sets. However, the ultra violet light still reaches the upper atmosphere above the photometer although there is no ultra violet light reaching the lower atmosphere (and no singlet delta production). Thus an ultra violet shadow is formed by the attenuation in the long atmospheric path lengths. There is no singlet delta due to ozone photolysis in this shadow. The second shadow is the absence of near infrared radiation from the sun that is scattered by the atmosphere to the ground. This radiation is less attenuated in the atmosphere than the ultra violet light and therefore has a lower shadow height. The center section of Figure 2.4 shows the near infrared light from the sun still reaching the atmosphere above the photometer although the ultra violet light has been fully attenuated. When both the ultra violet light and near infrared light do not reach the atmosphere above the photometer the

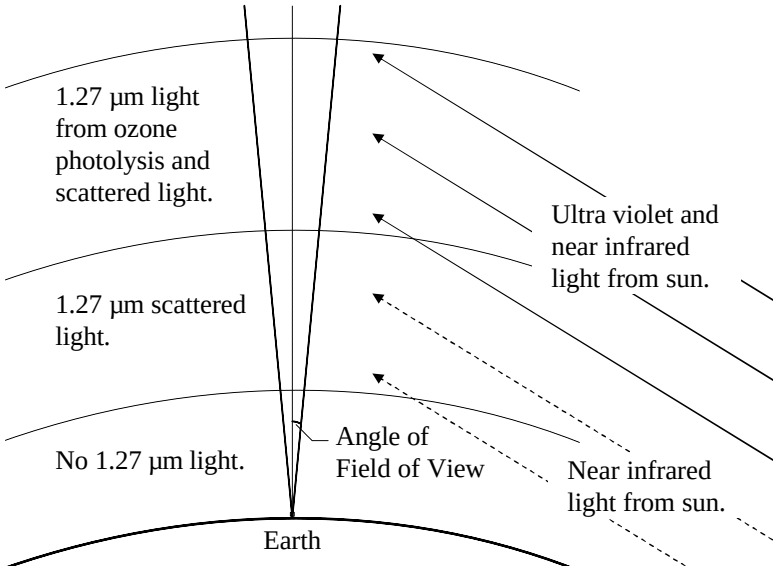

Figure 2.4: Viewing geometry and shadow heights of the two channel photometer looking from the ground up.

brightness at the ground from the entire vertical column is due to only the singlet delta emission and any airglow continuum. As the measured signal always contains a non singlet delta component it is necessary to develop a method to remove the contaminant signal.

2.5 The Two Channel Photometer

The actual two channel photometer uses a narrow band pass optical interference filter for the emission channel and a wide band pass optical filter for the background continuum channel. By using the two channels it is possible to determine the emission brightness even in the presence of a large background continuum.

For each channel the digital number output can be represented as follows:

$$\mathrm{DN} = k\left[\int B(\lambda)F(\lambda)\mathrm{d}\lambda + \int C(\lambda)F(\lambda)\mathrm{d}\lambda\right] \tag{2.7}$$

where k is the DN response to a given brightness level input [DN per $photon/cm^2/s/ster$], B is the emission brightness [$photons/cm^2/s/ster/nm$], C is the background continuum brightness [$photons/cm^2/s/ster/nm$] and F is the channel filter shape (which includes the optical filter and photodiode responsivity). The measured signal in each of the two channels (narrow and wide) of the photometer can be expressed as in equations 2.8 and 2.9, where B_o and C_o are the emission and continuum spectrum amplitudes respectively and B_s and C_s are the normalized emission and continuum spectrum shapes.

$$DN_N = k_N \left[B_o \int B_s(\lambda) F_N(\lambda) d\lambda + C_o \int C_s(\lambda) F_N(\lambda) d\lambda \right] \tag{2.8}$$

$$DN_W = k_W \left[B_o \int B_s(\lambda) F_W(\lambda) d\lambda + C_o \int C_s(\lambda) F_W(\lambda) d\lambda \right] \tag{2.9}$$

DN_N and DN_W are the measured values. The spectral shapes B_s, the emission spectrum transmitted to the ground (Figure 2.1), C_s, the Rayleigh scattered sunlight signal, F_N, the narrow channel filter shape, and F_W, the wide channel filter shape are all known. The narrow and wide channel calibration constants k_N and k_W respectively are determined during the instrument characterization. Therefore the values of B_o and C_o can be calculated from equations 2.8 and 2.9. The calculated B_o values represent the total column brightness of singlet delta detected at the ground.

The two channel photometer measurements made during twilight represent the variation in the total column brightness. As the sun sets the two shadow heights start at the ground and move up in altitude until the atmosphere is no longer illuminated. These twilight measurements can be used to determine the ozone profile and the singlet delta decay rate.

2.6 Ozone Retrieval

The actual method used to retrieve the ozone profile from the two channel photometer is a complex problem and beyond the scope of this thesis. A complete model

of the atmosphere and the associated radiative transfer are required to retrieve the ozone profile. However, the relationship between the measurements and the ozone concentration profile is demonstrated below.

As noted in section 2.5 the measurements from the two channel photometer can be used to determine the total column brightness of the singlet delta emission. This column brightness is the sum of the volume emission rates along the line of sight. At a given time, V_j represents the volume emission rate at altitude j and is equal to the product of the concentration (represented by [ ]) of singlet delta (O_2^* represents $O_2(a^1\Delta_g)$) and the probability of emission A (the Einstein spontaneous emission coefficient) divided by 4π (the steradian directional dependence), as given in equation 2.10 . The total column brightness B_o is given by equation 2.11, where α_j is the attenuation of the volume emission at altitude j to the ground and L_j is the vertical path length of the volume emission element at altitude j. This is the discrete representation of the total brightness integral shown in equation 2.6.

$$V_j = \frac{A[O_2^*]_j}{4\pi} \tag{2.10}$$

$$B_o = \sum_j V_j \alpha_j L_j = \sum_j \frac{A[O_2^*]_j}{4\pi} \alpha_j L_j \tag{2.11}$$

If it is assumed that the majority of the singlet delta emission is due to ozone photolysis (equation 2.2), a valid assumption at all altitudes during the day and twilight, then the rate of change of singlet delta can be expressed as the production rate through photolysis minus the loss rate through radiation and quenching as given in equation 2.12.

$$\frac{d[O_2^*]}{dt} = J_3[O_3] - [O_2^*](A + k_q[Q]) \tag{2.12}$$

where J_3 is the probability per ozone molecule of solar photolysis, A is the Einstein spontaneous emission coefficient, k_q is the quenching coefficient and [Q] is the concentration of quenching molecules. The two channel photometer measurements

yield the total column singlet delta emission brightnesses B_o which are intern used to determine the singlet delta concentrations ($[O_2^*]$). The radiative and quenching coefficients (A and k_q) are both known.

2.7 Singlet Delta Decay Rates

Although the retrieval of the ozone profile from the two channel photometer data is beyond the scope of this thesis it is possible to determine singlet delta decay rates, specifically for high altitudes, from the measured signal decay after the sun is no longer illuminating the atmosphere. In the absence of production the rate of change of singlet delta can be expressed as:

$$\frac{d[O_2^*]}{dt} = -[O_2^*](A + k_q[Q]) = -[O_2^*]\lambda \tag{2.13}$$

where $\lambda = (A + k_q[Q])$ is known. The concentration of singlet delta at a single altitude at any time t can be determined as follows.

$$\frac{1}{[O_2^*]} d[O_2^*] = -\lambda dt \tag{2.14}$$

$$\int_{[O_2^*]_o}^{[O_2^*]_t} \frac{1}{[O_2^*]} d[O_2^*] = -\int_{t_o}^{t} \lambda dt \tag{2.15}$$

$$\ln\left(\frac{[O_2^*]_t}{[O_2^*]_o}\right) = -\lambda t \tag{2.16}$$

$$[O_2^*]_t = [O_2^*]_o \, \mathrm{e}^{-\lambda t} \tag{2.17}$$

where $[O_2^*]_o$ is the concentration at time zero, λ is the combined quenching and radiative decay constant.

If the concentration of singlet delta at an integer time i is represented as $[O_2^*]_i$ then the volume emission rate for a given altitude j at time i is given as:

$$V_{i,j} = \frac{A[O_2^*]_{i,j}}{4\pi} \tag{2.18}$$

or

$$V_{i,j} = \frac{A[O_2^*]_{o,j}}{4\pi}\ \mathrm{e}^{-\lambda i} \tag{2.19}$$

The total brightness B_i measured at the ground at time i is the sum of the volume emission rate from each altitude j along the line of sight.

$$B_i = \sum_j V_{i,j}\alpha_j \mathrm{L}_j = \sum_j \frac{A[O_2^*]_{o,j}}{4\pi}\ \mathrm{e}^{-\lambda_j i}\ \alpha_j \mathrm{L}_j \tag{2.20}$$

Once production of singlet delta has stopped the emission decays from the lower altitudes upwards, this is demonstrated in Figure 2.5 by the altitude profiles measured with OSIRIS near the equatorial region. Therefore the change in brightness detected at the ground can be approximated with reasonable accuracy by the decay of the singlet delta vertical profile peak which starts at a low altitude and moves to higher altitudes during evening twilight. If the decay of singlet delta is assumed to be dominated by the peak altitude at each time then the altitude dependent total decay time constant λ_j in equation 2.20 can be written as a time dependent decay constant λ_i, as in equation 2.21. For the assumption that the total decay time constant at time i is the same as the total decay time constant for the corresponding weighted emission altitude j equation 2.20 can be simplified to:

$$B_i = \frac{A\,[O_2^*]_o}{4\pi}\ e^{-\lambda_i i}\ \alpha_i \tag{2.21}$$

where i represents time, λ_i is the total decay time constant at time i and α_i is the attenuation of the singlet delta emission to the ground at time i (which corresponds to the weighted altitude of the singlet delta peak at time i).

With this assumption it is possible to solve for the total decay time $(1/\lambda_i)$ using the TOP2000 measured data. Once production has stopped and the background signal has become small, the narrow channel DN is proportional to the emission brightness. Taking the natural log of equation 2.21 gives

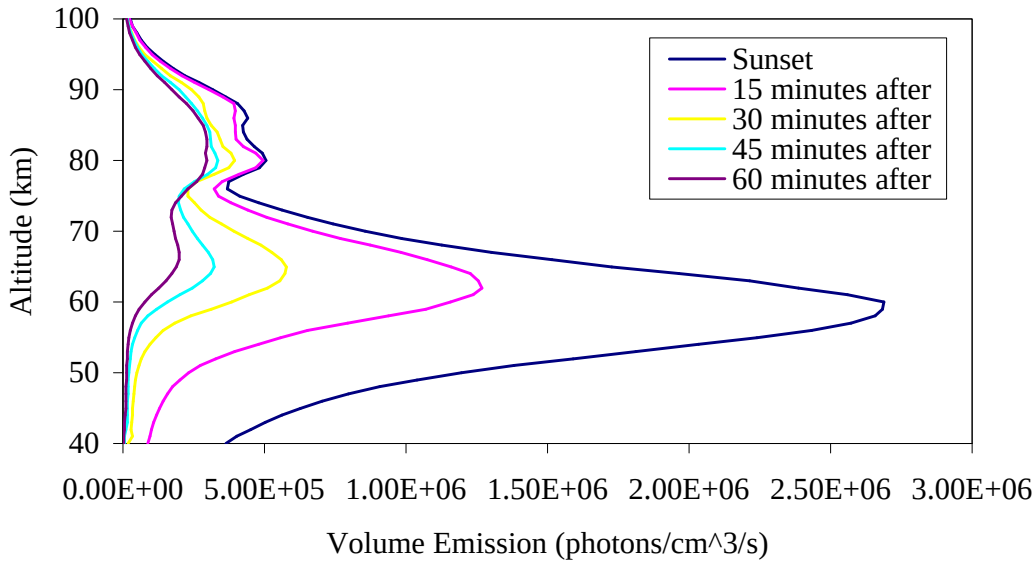

Figure 2.5: Singlet delta altitude profiles at different times past sunset as measured by OSIRIS (August 15, 2002).

$$\ln\left(B_i\right) = -\lambda_i i + \ln\left(\frac{A\left[O_2^*\right]_o}{4\pi}\ \alpha_i\right) \tag{2.22}$$

During the time period when the adopted assumptions are valid the slope of the natural log of the narrow channel DN vs time plot will give the total decay time constant λ_i. These measured decay times $(1/\lambda_i)$ can be compared to known values in order to validate the two channel photometer measurements.

2.8 Summary

A brief history of singlet delta measurements and the important photochemistry involved in the production and loss of the 1.27 μm emission have been discussed. The two channel photometer technique and its ability to provide ozone retrievals and, more importantly for this thesis, calculate the singlet delta decay rates were also examined.

Chapter 3

Design and Implementation

3.1 Introduction

The two channel photometer TOP2000 is a modified version of the original 1.27 micron photometer described by Evans [23] and a continuation of the proof of concept design by How [16]. The front end optical system is unchanged. However, the original PbS photoconductors have been replaced with InGaAs photodiodes for improved signal to noise characteristics. In this chapter each section of the TOP2000 instrument and its overall functionality are described. The optical system was taken directly from a previous two channel photometer. Each of the electronic blocks (with the exception of the lock-in amplifiers), the assembly code and C programs were designed, constructed and implemented in house.

3.2 PbS vs InGaAs

Replacing the previously used lead sulphide (PbS) detectors with indium gallium arsenide (InGaAs) photodiodes improved the overall noise performance of the two channel photometer. The noise equivalent power (NEP) is defined as the optical signal power required to generate a photocurrent that is equal to the total noise

current (a signal to noise ratio equal to one) at a given frequency and a bandwidth of 1 Hz. Typical values of NEP for PbS detectors are of the order of 1x10^{-12} $W/\sqrt{Hz}$ while typical NEP values for InGaAs detectors are of the order of 1x10^{-14} $W/\sqrt{Hz}$. Thus the use of InGaAs photodiodes should improve the NEP of the two channel photometer by two orders of magnitude. Therefore, the InGaAs photodiodes can measure much lower light levels before reaching a S/N ratio of 1 or, at the same input light power, the InGaAs detector has inherently less noise.

3.3 Design Specifications

The design objective of the two channel photometer was to measure the singlet delta and the background continuum emission brightness at 1.27 microns over the complete range of atmospheric signal levels during a twenty four hour period. In addition the photometer had to be able to operate in a cold environment (Eureka, NU ambient temperature during the spring and fall could vary between -10 to -50 degrees Celsius). The gain control, data collection and data storage were to be interfaced with a computer. During late twilight and nighttime the signal levels are very low, this is apparent from the volume emission profiles sixty minutes after sunset shown in Figure 2.5. Therefore, a method to recover signals with large noise components was necessary. Based on the previous photometers design the method of recovering the amplitude of a modulated signal through a lock-in amplifier was used. The purchased lock-in amplifiers would also provide the proper gain control to cover the several orders of magnitude brightness variation during an entire day. Initial twilight testing showed that a pre-amplifier with a current to voltage gain of 10^6 followed by a second stage voltage gain of 100 was appropriate for the dynamic range gain of the purchased lock-in amplifiers.

3.4 Overall System

The overall system block diagram is shown in Figure 3.1. The front end optical system (Figure 3.2) is basically unchanged from the original design described by Evans [23]. The light entering the photometer is focused, modulated by the shutter action of the optical chopper, split and filtered before reaching the InGaAs photodiodes. The light for each channel is focused on to a InGaAs photodiode that converts the photon energy into an electrical signal. The modulated electrical signal, at the frequency of the optical chopper, is amplified by a transimpedance pre-amplifier stage. A lock-in amplifier is used to demodulate the pre-amplifier output producing a DC output signal that is proportional to the modulated amplitude of the pre-amplifier signal. The DC signal from the lock-in amplifier that represents the signal brightness is converted to a digital number and sent for storage on a computer through the computer interface.

3.5 Optical System

The optical system for the TOP2000 photometer is shown in Figure 3.2. Out of field scattered light is minimized by the baffle system. The main baffle entrance aperture is focused by the objective lens on to the entrance aperture for the first condensing lens. The first condensing lens entrance aperture in the original 1.27 μm photometer defined the 5 degree field of view [7]. The field of view in the TOP2000 photometer however is defined by the InGaAs photodiode size reducing the field of view to approximately 2°. The first condensing lens focuses the light to a spot that is modulated by the tuning fork chopper. The modulated light passes through the second condensing lens which expands the light to be approximately parallel. This near parallel light is filtered by the optical wide band interference filter that also acts as the blocking filter for the optical narrow band filter. The modulated, filtered light is then split by a 45 degree non-polarizing beam splitter made from

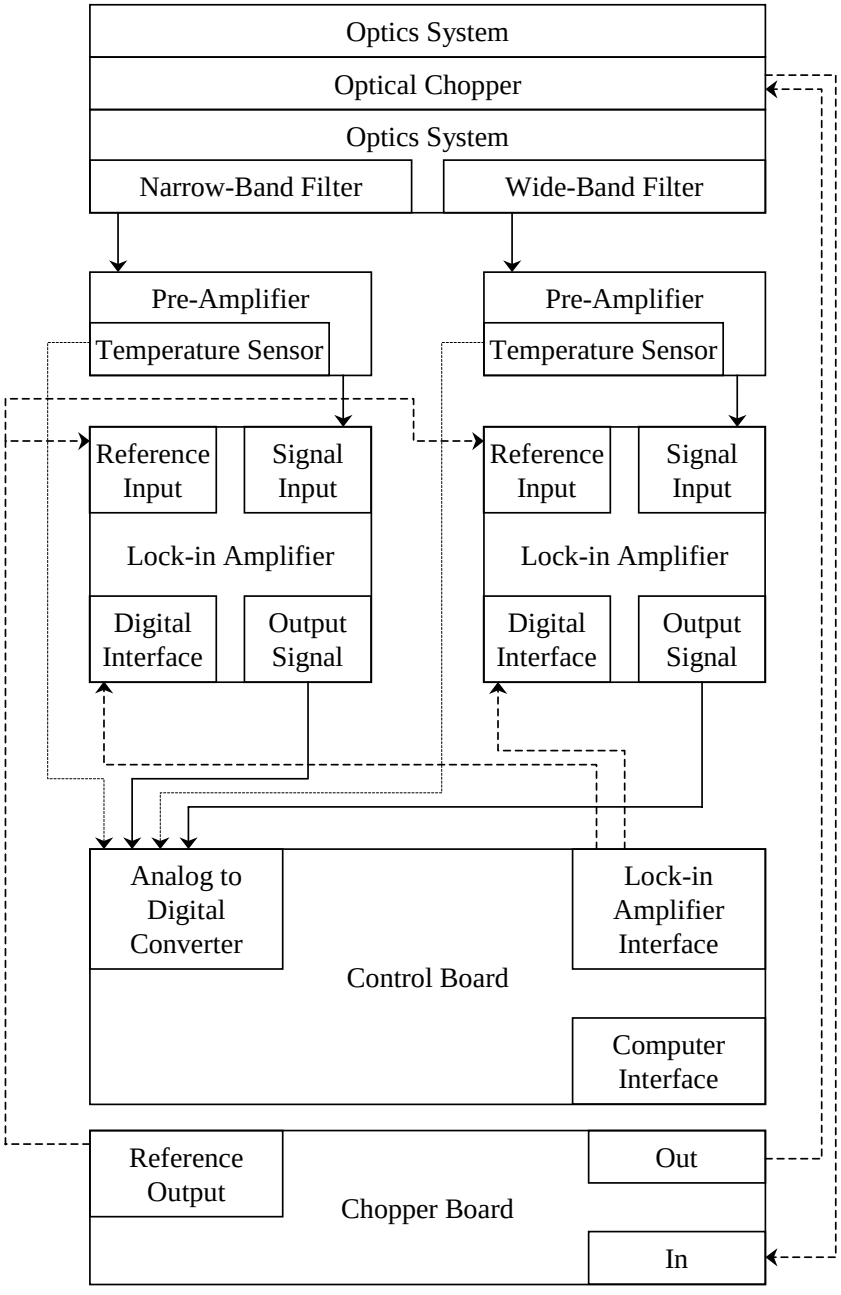

Figure 3.1: Block Diagram of TOP2000

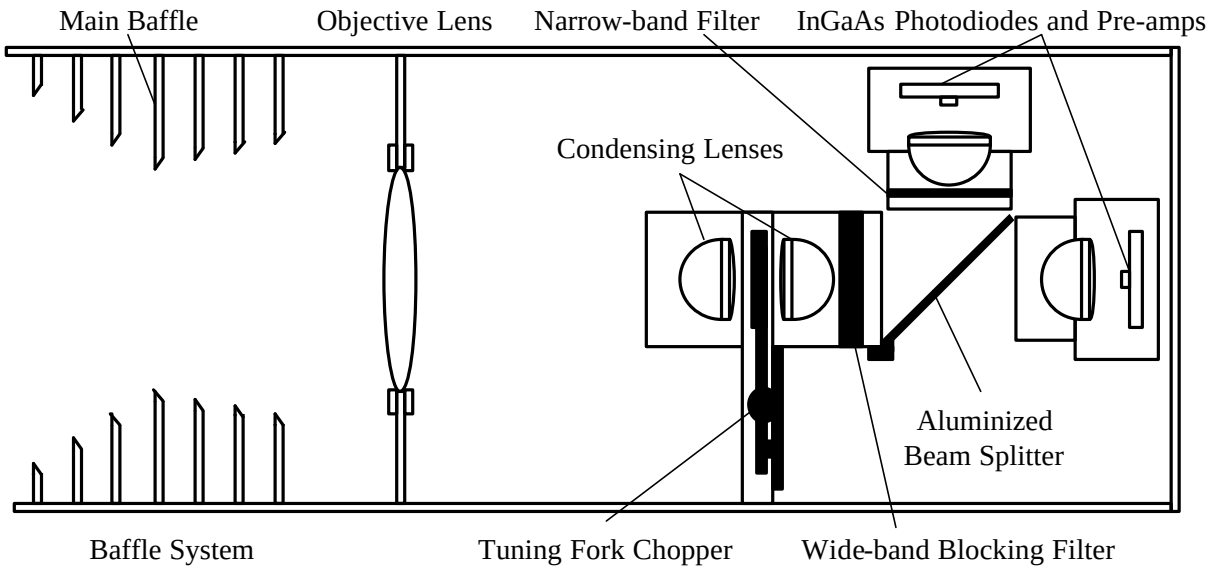

Figure 3.2: Optical System Schematic

aluminized Lucite for 90% reflection and drilled holes to give 10% transmission. The 90% reflected light is filtered by the narrow band interference filter and focused by a condensing lens on to a InGaAs photodiode for the narrow band channel. The 10% transmitted light is focused on to a InGaAs photodiode for the wide band channel. The narrow band and wide band filter bandwidths are such that the beam split ratio (90% to the narrow channel and 10% to the wide channel) provides approximately equal power to the narrow and wide channel photodiodes for a flat spectrum input.

3.6 Electronics

3.6.1 The InGaAs Photodiode

The light in each channel is converted into an electrical signal by the InGaAs photodiodes through photogeneration, the process of absorbing a photon with sufficient energy to create electron hole pairs (EHPs). Figure 3.3 shows the generated electron

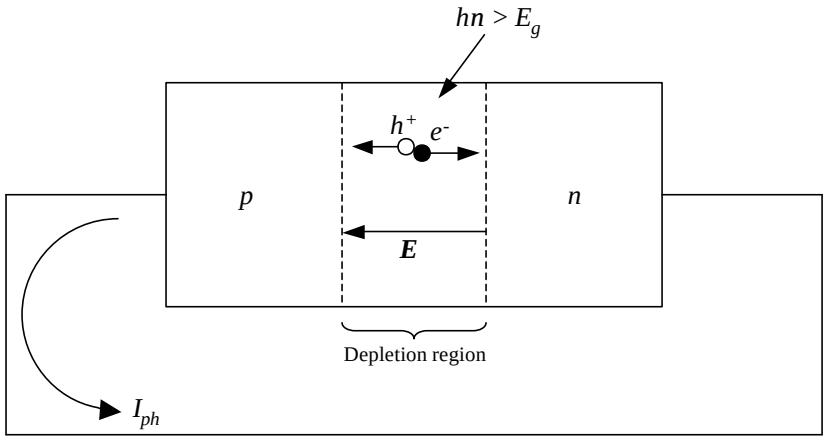

Figure 3.3: Photodiode electron hole pair generation from incident photon.

hole pair within the depletion region of a photodiode for an incident photon with energy greater then the bandgap energy (E_g) of the material. The generated charges within the depletion region drift with the electric field (E) that is setup up at the pn junction producing a photocurrent I_{ph}.

The efficiency at which the EHPs are generated for a given number of incident photons is the quantum efficiency (QE) η, this is defined as the number of electrons collected per second over the number of photons arriving per second as described in equation 3.1 [24] (P_o is the incident optical power).

$$\eta = \frac{I_{\mathrm{ph}}/e}{P_{\mathrm{o}}/\mathrm{h}\nu} \tag{3.1}$$

The wavelength dependence of the quantum efficiency affects the generated photocurrent per incident optical power or the responsivity (R) is given by equation 3.2 [24].

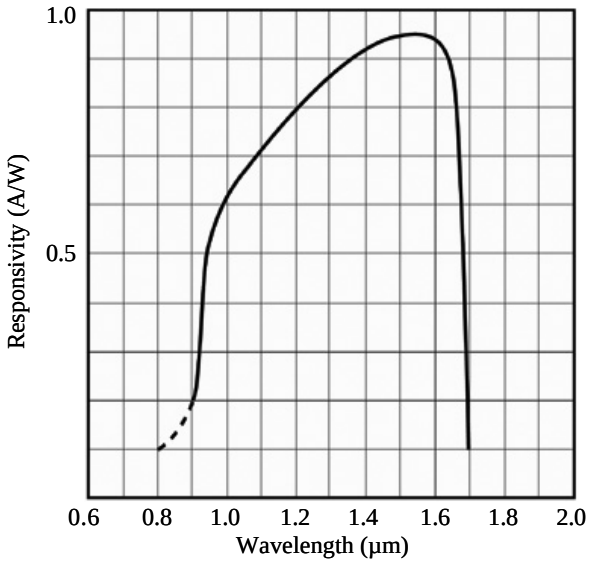

Figure 3.4: InGaAs Photodiode Responsivity

$$R = \frac{I_{\text{ph}}}{P_{\text{o}}} = \eta \frac{e\lambda}{hc} \tag{3.2}$$

The spectral responsivity (at T=25°C) for the 1mm active area diameter Hamamatsu G8370 series InGaAs photodiodes used in TOP2000 is shown in Figure 3.4. The responsivity curve has a filtering effect on the spectrum of incident light.

In the pre-amplifier design the photodiode is reversed biased so that the output current is linearly proportional to the input illumination. Reverse biasing a photodiode increases the depletion region width, which in turn increases the temperature dependent noise from randomly generated electron hole pairs due to the larger volume. However compared to no biasing, reverse biasing eliminates the possibility of non-linear photocurrents from forward biasing due to noise offsets from the operational amplifiers.

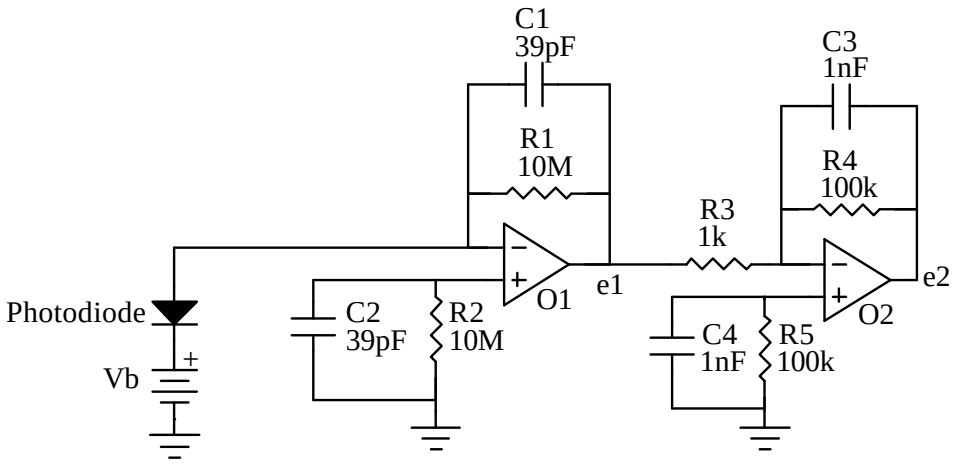

Figure 3.5: Pre-Amplifier

3.6.2 Pre-Amplifiers

Both pre-amplifiers in the photometer follow the two stage amplifier design shown in Figure 3.5. The circuit board layout for the pre-amplifiers was designed in Trax-Maker and then given to the University of Saskatchewan Electrical Engineering technicians office for production.

The first transimpedance stage has a voltage output equal to the input photocurrent multiplied by the feedback resistor ($R_1 = 10M\Omega$) as ideally described in Equation 3.3.

$$e_1 = -I_{ph}R_1 \tag{3.3}$$

To prevent high frequency oscillations due to the non-ideal open loop response of the operational amplifier a 39pF bypass capacitor (C_1) was placed in parallel with R_1. The first order low pass filter feedback has a cutoff frequency of 408 Hz. To reduce the output offset error and compensate for thermal noise from the feedback

resistor R_1, a resistor of equal value ($R_2 = 10M\Omega$), that is capacitively bypassed to remove its high frequency noise, is connected to the non-inverting input of the operational amplifier. The first stage output voltage is amplified 100 times by the second stage inverting amplifier.

3.6.3 Temperature Sensors

Each pre-amplifier board has a temperature sensor that is located physically close to the photodiode. Both sensors are low power MAX6611 surface mount chips with an accuracy to measure temperature within $\pm 1°C$. The sensor TEMP pin provides an analog output that is given by the linear function of the die temperature in Equation 3.4

$$V_{TEMP} = 1.2V + (T°C \times 16mV/°C) \tag{3.4}$$

Self heating is minimal under normal operating conditions. At 50°C and maximum current operating conditions the increase in die temperature from power dissipation is only 0.4°C.

3.6.4 Chopper Board

The chopper board contains the positive feedback oscillator circuit that interfaces with the tuning fork optical chopper, the reference output and the analog power and ground for both lock-in amplifiers. The tuning fork chopper oscillator circuit is shown in Figure 3.6. The two coils represent the drive and pickup coils of the tuning fork chopper. A push button (S1) provides a step input to the drive coil to initiate oscillation when power on startup conditions fail. The tuning fork has very high Q bandpass filter characteristics at 200Hz that provides both a stable reference output for the lock-in amplifiers and a stable modulation of the incoming light. The output of the oscillator circuit is fed to a buffer that connects to both lock-in amplifiers reference inputs. To eliminate problems with high frequency oscillations the buffer

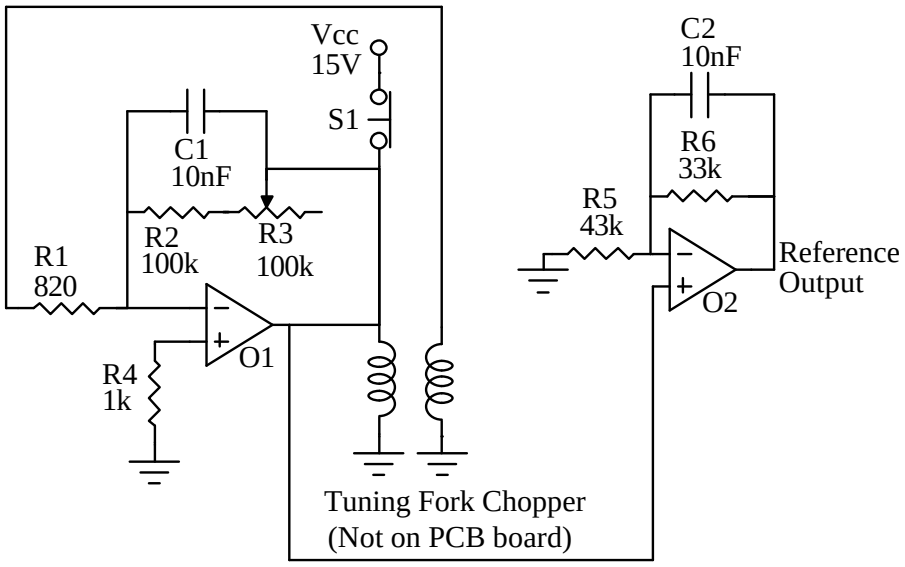

Figure 3.6: The Chopper Circuit

is a non-inverting amplifier with D.C. gain attenuation of 23 percent and first order low pass filtering with a cutoff frequency of approximately 3kHz.

3.6.5 Lock-in Amplifiers

The main principle used by lock-in amplifiers to recover signals with a large noise component is demodulation of an amplitude modulated input signal. Demodulation is the process of recovering the required signal from a carrier wave. If the amplitude A_i, equation 3.5, is the signal of interest and $sin(\omega t)$ is the carrier wave then multiplying S_i by a reference signal S_r with the same frequency as the carrier allows for the recovery of A_i. Equation 3.7 shows the result of multiplying the carrier wave by a reference wave (equation 3.6). The carrier wave and reference wave have the same frequency ω, and ϕ represents the phase difference between the two waves.

$$S_i = A_i sin(\omega t) \tag{3.5}$$

$$S_r = A_r sin(\omega t + \phi) \tag{3.6}$$

$$S = \frac{A_i A_r}{2} cos(\phi) - \frac{A_i A_r}{2} cos(2\omega t + \phi) \tag{3.7}$$

Equation 3.7 represents the output of the demodulator in a lock-in amplifier. With further processing, such as ensuring the phase difference between the two waveforms is zero and low pass filtering the demodulator output to eliminate the 2ω term, the signal of interest (A_i) is recovered. The lock-in amplifiers used for this project were purchased from Scitek Instruments. The functional block diagram for the Scitek lock-in amplifier is shown in Figure 3.7. If the signal, $s(t)$, and reference, $r(t)$, inputs are as given by equations 3.8 and 3.9, where V_s and V_r are the signal and reference rms voltage amplitudes, ϕ is the phase difference between the signal and reference at frequencies ω_s and ω_r, then the output signal after the multiplication of the two inputs and low pass filtering is given by equation 3.10. In the photometer the frequencies ω_s and ω_r are equal to 200 Hz.

$$s(t) = \sqrt{2} V_s sin(\omega_s t) \tag{3.8}$$

$$r(t) = \sqrt{2} V_r sin(\omega_r t + \phi) \tag{3.9}$$

$$v_o(t) = V_s V_r cos(\phi) \tag{3.10}$$

If the reference and signal are in phase ($\phi = 0$) and V_r equals 1 then the output of the lock-in amplifier is the rms value of the input sine wave (V_s). If the amplitude of the sine wave input signal varies slowly with respect to the modulating frequency then the variations of the DC lock-in amplifier output represent the amplitude variations of the input signal.

The Scitek lock-in amplifiers signal inputs are obtained from the respective preamplifiers via a shielded cable. Both lock-in amplifiers use the same reference signal

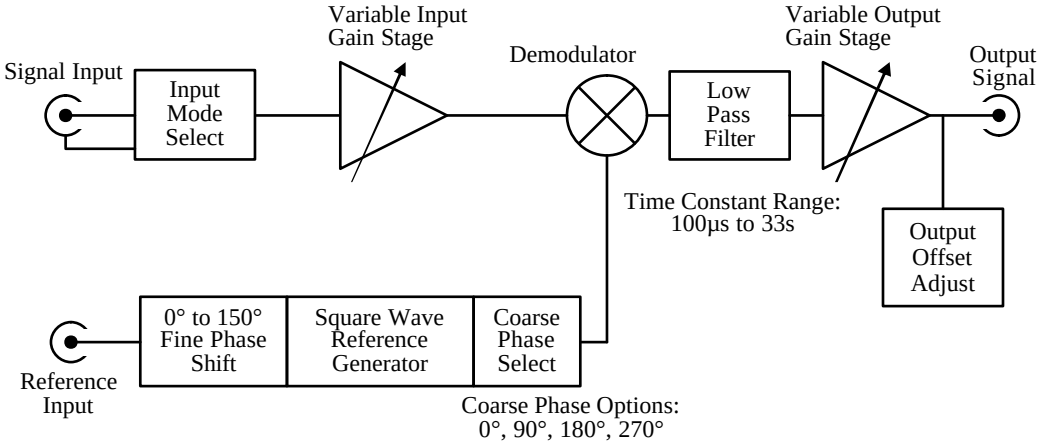

Figure 3.7: Scitek 432 Lock-in Amplifier Block Diagram

input from the chopper board. The output of each lock-in amplifier is connected to an input channel of the analog to digital converter.

Each lock-in amplifier is connected to the microcontroller through a 34 pin IDC connector. This interface allows software control of the lock-in amplifier settings for the input mode (single ended or fully differential and AC or DC coupled), input gain, output gain, low pass filter time constant, coarse and fine phase adjustment and the lock-in output offset adjust.

3.6.6 Control Board

The control board main components are the microcontroller, analog to digital converter, and an RS232 driver/receiver. The block diagram is shown in Figure 3.8. The microcontroller is an Atmel AT89S53 processor based on the industry standard 8051 architecture. It initiates and collects data from the analog to digital converter, writes control data to the lock-in amplifiers, sends data to and receives commands from a computer over the RS232 data line. Communication to the analog to digital converter is done through the SPI serial interface (an alternate function of port 1).

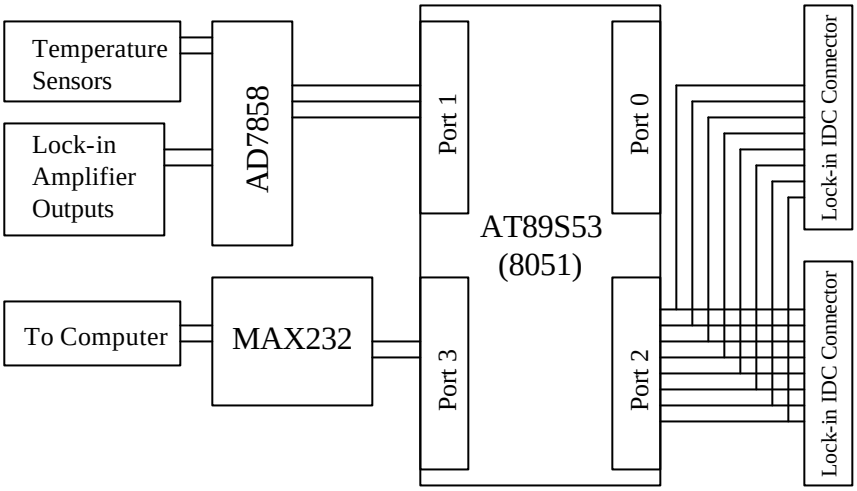

Figure 3.8: Control Board Block Diagram

Commands and data are received and transmitted through the serial channel in port 3. Port 2 is interfaced with the lock-in amplifiers.

The Analog Devices AD7858 12 bit sampling analog to digital converter receives four inputs, two temperature sensor output voltages and lock-in amplifier output voltage. The MAX232 line driver/receiver provides the proper interface between the microcontroller and the computer for RS232 communication.

3.6.7 Power Supply

A Power-One 16 watt (HTAA-16W-A) linear power supply is used to provide 5V, +15V and -15V DC voltages from the 120V, 60Hz line voltage. Three AA batteries in series provides a clean 4.5V DC supply. Both the batteries and power supply are housed separately from TOP2000 in a shielded case. The supply voltages and the digital and analog grounds are connected to TOP2000 by shielded cables.

3.7 Software

3.7.1 Microcontroller

The Atmel AT89S53 microcontroller program, written in assembly language, provides the necessary logic to communicate with the computer, the analog to digital converter and to program the lock-in amplifiers. The assembly code program was loaded into the microcontroller using the EE AT89S53 evaluation board (#7). Data sampling is initiated by the computer over the RS232 communication line. Following the receipt of the command the microcontroller initiates the A/D and cycles through all four channels to obtain the two lock-in amplifier values and the two temperature sensor values. All four data values are stored in the microcontrollers RAM and sent to the computer. At this point the data sample is completed until the computer initiates a new cycle.

3.7.2 CPU

Communication between the control computer and the TOP2000 photometer was through software written in C. The design and development of the software for TOP2000 is described in the following. The CPU software controlled the rate of data collection, lock-in amplifier settings and data storage. The data were stored in subdirectories named by the day collection started. The data files were named according to the first data sample time stamp. A new data file was created every two hours. Each line in a data file contains 21 fields as described in Table 3.1. All fields are decimal values. Each sample is time stamped when the data are received from TOP2000. The time field is the value of the computer clock in seconds past 00:00:00 January 1, 1970 concatenated with the number of milliseconds past the second. The lock-in amplifier settings are the decimal values of the binary codes given to each lock-in amplifier at the time of setup and represent the gain, phase and offset values. The input and output gain settings for the lock-in amplifiers are user entered before

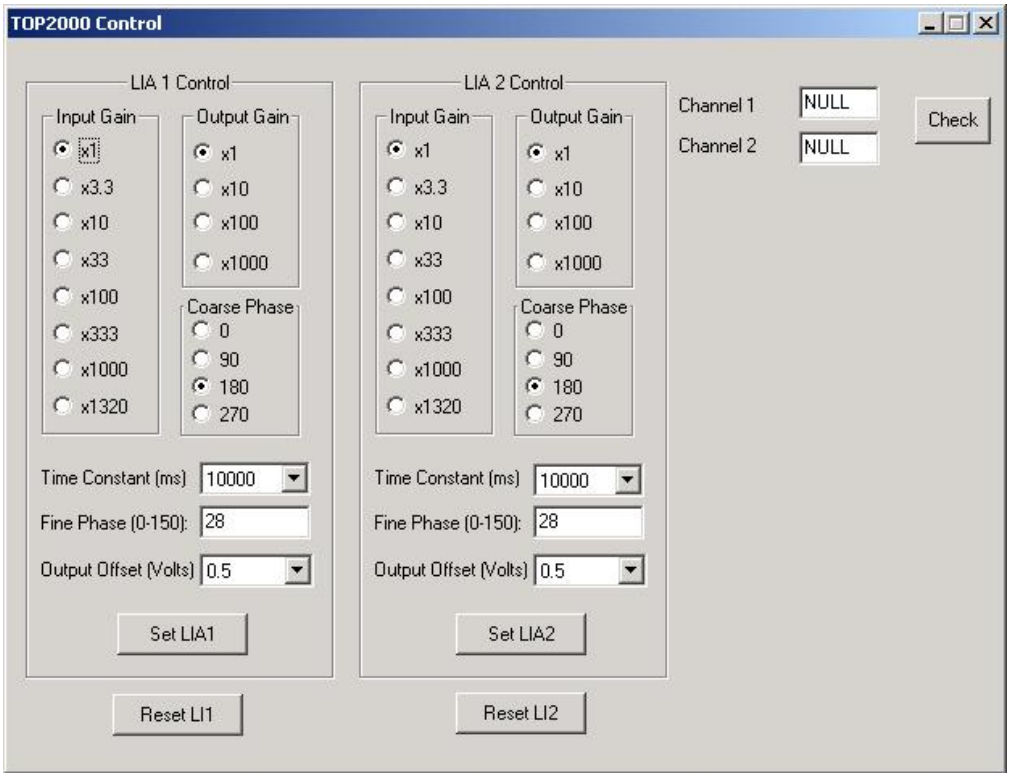

Figure 3.9: TOP2000 Graphical User Interface

data collection starts. The other settings must be manually changed in the code if the lock-in amplifier phase, time constant and offset settings change from those determined most suitable. The lock-in amplifiers are manually controlled through a graphical user interface shown in Figure 3.9. The lock-in amplifier settings are entered or selected for each channel in the graphical user interface. The settings for each channel are transmitted to TOP2000 by pressing the corresponding Set LIA button. Both lock-in amplifiers output, in volts, can be seen by pressing the Check button (this button can not be used when the TOP2000 is collecting data). The Reset LIx clears the lock-in amplifiers registers and sets the lock-in to a low gain base case. Both the check and reset buttons are used for testing and are not required for normal operation of TOP2000.

Table 3.1: Text File DataFields

Field	Value
1	Channel 1 Signal Upper Byte
2	Channel 1 Signal Lower Byte
3	Channel 2 Signal Upper Byte
4	Channel 2 Signal Lower Byte
5	Integer Time
6	Channel 1 Temperature Upper Byte
7	Channel 1 Temperature Lower Byte
8	Channel 2 Temperature Upper Byte
9	Channel 2 Temperature Lower Byte
10	Channel 1 Lock-in Amplifier Input Gain
11	Channel 1 Lock-in Amplifier Output Gain
12	Channel 1 Lock-in Amplifier Time Constant
13	Channel 1 Lock-in Amplifier Coarse Phase
14	Channel 1 Lock-in Amplifier Fine Phase
15	Channel 1 Lock-in Amplifier Offset
16	Channel 2 Lock-in Amplifier Input Gain
17	Channel 2 Lock-in Amplifier Output Gain
18	Channel 2 Lock-in Amplifier Time Constant
19	Channel 2 Lock-in Amplifier Coarse Phase
20	Channel 2 Lock-in Amplifier Fine Phase
21	Channel 2 Lock-in Amplifier Offset

3.8 Environmental Housing

In order to operate TOP2000 in a cold environment a heated, well insulated box was constructed. The box was insulated with two layers of 2.5 inch R7.5 insulation and a half inch thick quartz window transmitted the sky radiation through to the TOP2000 instrument. A thermostatically controlled 150 watt strip heater was placed close to a continuously blowing computer fan. The air from the fan was directed towards the quartz window in order to prevent frost build up. Both the TOP2000 and the power supply were housed within the box. Power and communication were provided by cables that entered through a small hole in the side of the box. A 120 volt light socket was mounted within the box to provide a test light. The 25 watt light bulb used could be turned on and off by a switch wired externally to the box in an environmental casing. Modifications to the box were made following the first Eureka, NU campaign in the fall of 2003. As discussed in Chapter 5 better temperature control and the ability to get a 'zero' reference were needed. These measurements were met through the addition of a PID controller and strip heater to provide better temperature stability and, a shutter system provided an intermittent dark signal throughout the observations.

3.9 Images of TOP2000

The major part of the time spent on this research project was associated with the construction of TOP2000. The completed photometer is shown inside the environmental box in Figure 3.10. The main baffling and the objective lens are contained within the top narrow diameter portion of TOP2000. The wider diameter case contains the remaining optical elements, the tuning fork chopper and pre-amplifiers. The square casing at the bottom of TOP2000 contains the lock-in amplifier, the control and chopper circuit boards. The tanned colour box below TOP2000 houses the power supply. The environmental box also includes the strip heater, fan and

air flow control tubing together with the thermostat controller and 120 volt power outlets. Figure 3.10 also shows TOP2000 operating within the environmental box at Eureka, NU. The instrument setup was strapped to the pallets, which were weighted down, with the blue tie downs to prevent it from blowing over during the frequent wind storms.

The major components of the optics system, outlined in Figure 3.2, are shown in Figure 3.11. The elements that can be seen are the first condensing lens, which focuses the light from the objective lens to a spot. The drive and pickup coil of the tuning fork chopper are visible together with the joint end of the tuning fork. The pre-amplifiers, which are mounted close to the photodiodes, are housed in an aluminum casing to minimize stray light on the detectors and to prevent electrical noise pickup. The light passing through the beam splitter is focused on to the photodiode of the wide channel pre-amplifier. The reflected light from the beam splitter goes to the narrow channel photodiode, not visible in this figure.

3.10 Summary

The design specifications and overall design of the two channel photometer have been discussed. Each component of the overall design block was described in detail. All of the electronics and described software, with the exception of the lock-in amplifiers that were purchased, was designed and constructed for the photometer.

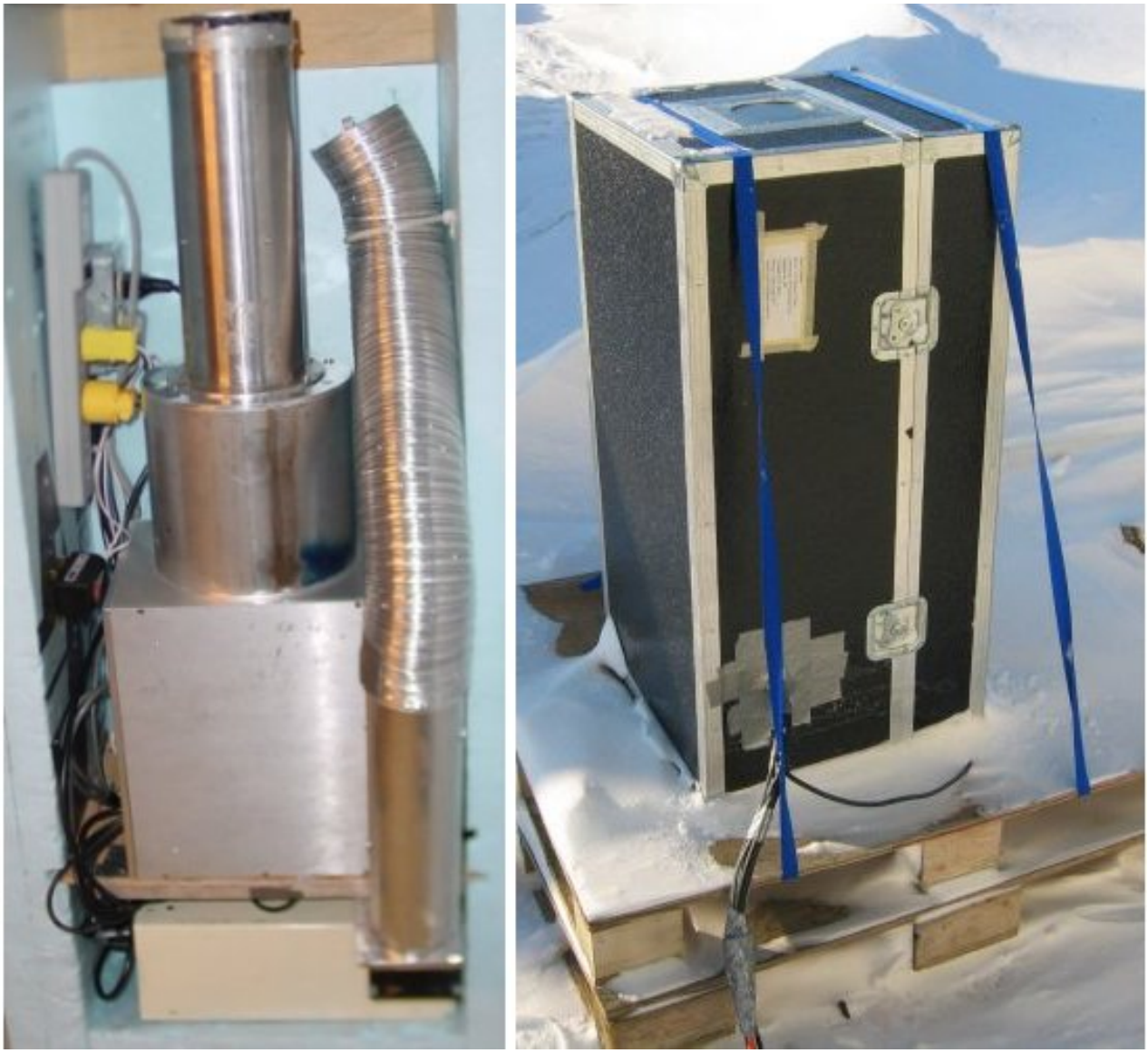

Figure 3.10: TOP2000 setup in the environmental box and operating at Eureka, NU.

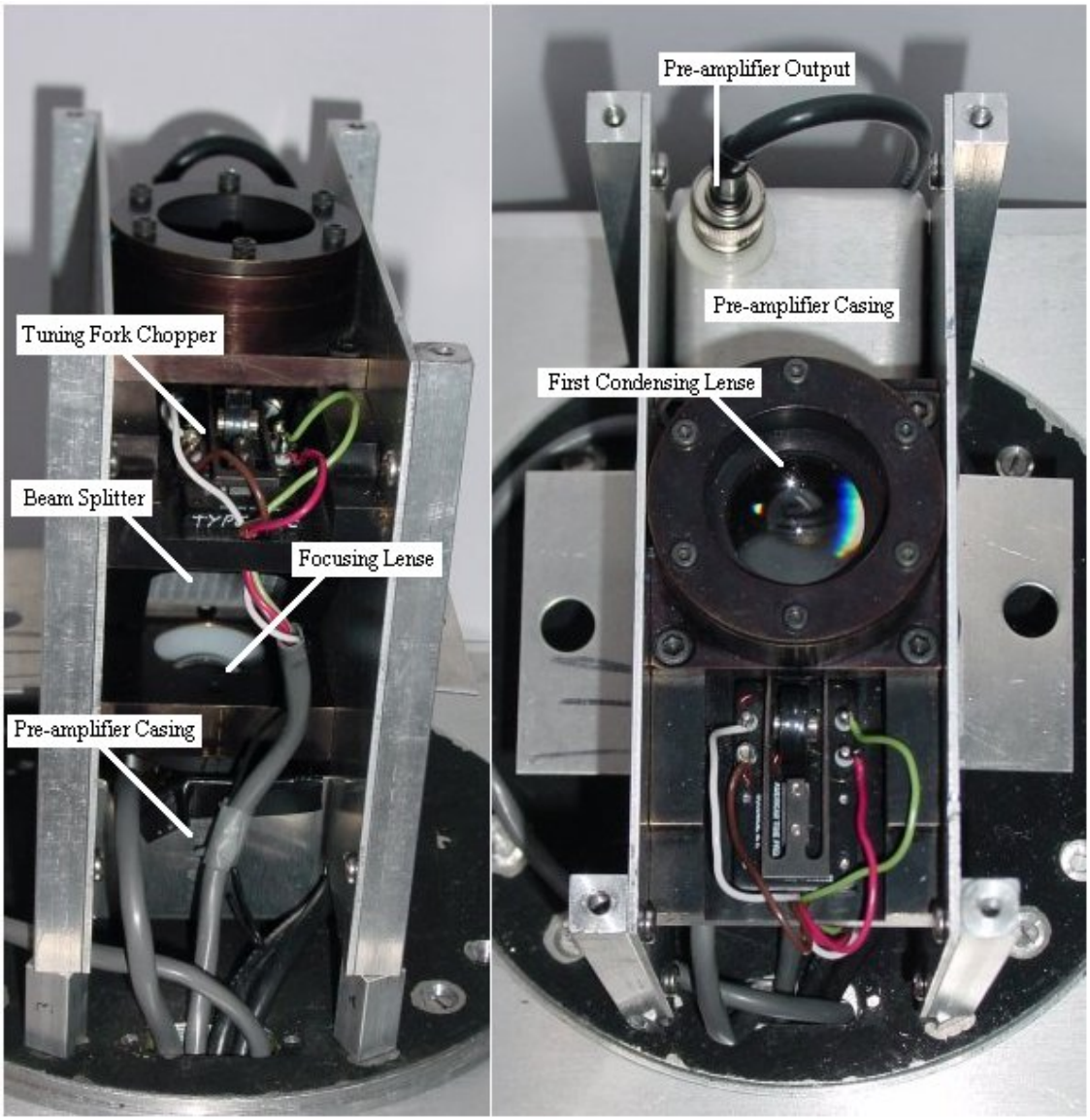

Figure 3.11: The optical system of TOP2000.

Chapter 4

Testing and Calibration of TOP2000

4.1 Introduction

During the construction of TOP2000 each block component was tested individually. This section describes the characteristics of the system as a whole. The performance of TOP2000 is given, specifically the output offset characteristics, temperature stability and noise characteristics. Both the wavelength calibration and absolute brightness calibration of TOP2000 are also presented.

4.2 Observed Output Offset Characteristics

The dark output offset is the recorded data level when there is no light input to the photometer. Under absolutely stable conditions the output offset would remain constant and could be easily removed from the data to leave only the desired signal levels. However, the output offset varies with changes in the lock-in amplifier gain, lock-in amplifier phase, and temperature.

4.2.1 Lock-in Amplifier Settings

Prior to connecting the lock-in amplifiers to the associated pre-amplifier and analog to digital converter two potentiometer adjustments were made in order to minimize each lock-in amplifiers internal offsets.

First the DC offset from the lock-in amplifier components before the demodulator stage, shown in Figure 3.7, was minimized. At high gain settings and with a short low pass filter time constant this DC offset appears at the output of the lock-in amplifier approximately as a square wave. A 200 Hz sine wave reference, generated by a function generator, was connected and the signal input was left unconnected. The input and output gain were set at maximum (x100 input and x1000 output) and the filter time constant after the demodulator was set to its minimum (0.1 micro seconds). The throughput trim pot on the lock-in amplifier was adjusted to minimize the output ripple as viewed on an oscilloscope. This was done for both lock-in amplifiers.

Second the DC offset from components after the demodulator was minimized. A 200 Hz sine wave, again from a function generator, was connected to the lock-in amplifier reference signal and the lock-in amplifier signal input was left unconnected. The output was observed on an oscilloscope. The lock-in amplifier was set at maximum gain (x100 input and x1000 output) with a 1 second filter time constant. The offset trimpot on the lock-in amplifier was adjusted for the minimum output offset. This was done for both lock-in amplifiers.

To allow the analog to digital converter to measure fluctuations in the output of the demodulated DC signal level that might go negative an output offset adjust of 0.5 volts was set at the output of the lock-in amplifiers (output offset adjust in Figure 3.7) as the 'zero' reference voltage.

4.2.2 Output Offset vs Lock-in Amplifier Phase

As explained in Chapter 3 the lock-in amplifier output is sensitive to the phase difference between the input signal and reference signal. The reference phase shift that provides maximum signal output for each lock-in amplifier was determined by attempting to null the output with a given signal brightness input. The null point represents a 90° phase difference between the modulated signal and reference inputs of the lock-in amplifier. This phase shift gives zero signal after the demodulator. By adding 90° to the null phase point the maximum signal output is acquired.

The phase settings for each lock-in amplifier of TOP2000 that minimized the difference between the modulated signal from the pre-amplifier and the reference output from the optical chopper circuit (Figure 3.6) were determined in the laboratory. The actual null phase setting had to be determined using lower gain settings due to the large changes in the output offset level at high gain caused by even small changes in phase. With a light source input to TOP2000 the coarse phase was set for a positive increase in DN with increasing light brightness input. This coarse phase setting was then adjusted by 90 degrees in order to find the null point by adjusting the fine phase. The fine phase was tuned to minimize the output offset difference from the 0.5 volt reference value. Once the minimum value had been determined a 90° coarse phase change was added.

For perfectly random noise output from the pre-amplifier, phase adjustments to the lock-in amplifier with no input light to the TOP2000 should not change the DN of the output offset. However, during laboratory testing of TOP2000 it was noticed that the dark output offset had a dependence on the lock-in amplifier phase setting. With the TOP2000 at the highest gain setting there were large changes in the dark output offset for even small changes to the fine phase setting of either lock-in amplifier. The dark output offset changes for different coarse phase settings at the lowest gain (x1 input and x1 output) are shown in Figure 4.1. Determining the best phase settings for the lock-in amplifiers became an iterative process during both the laboratory and twilight measurements. The optimum lock-in amplifier

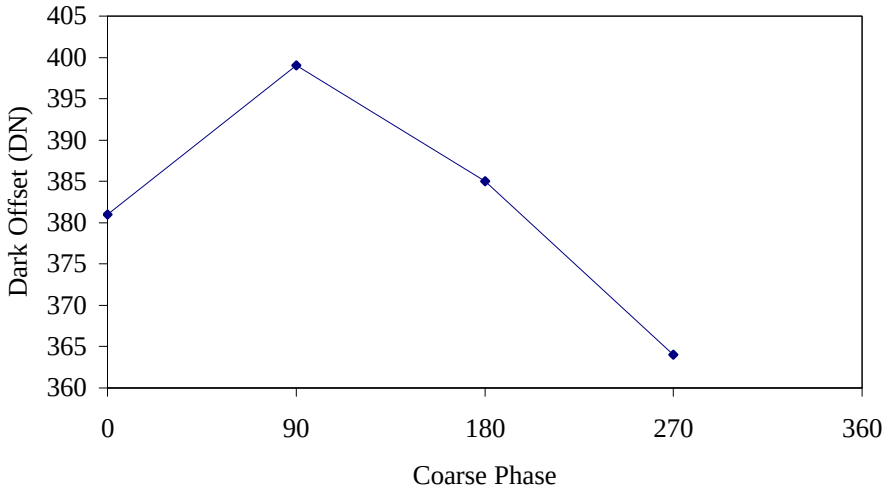

Figure 4.1: Dark output offset vs coarse phase at low gain.

coarse and fine phase settings for TOP2000 are 180° and 28° respectively for both channels.

4.2.3 Output Offset vs Lock-in Amplifier Gain Settings

During measurements of the airglow twilight decay different gain settings are required for the lock-in amplifier as the brightness decreases. The increased gain allows low level signals to be detected although the dark output offset increases with increasing gain setting. This dark output offset for different gain settings was measured with TOP2000 in a controlled environment (constant temperature). The variation in the output offset for both channels at three different gain settings (x1, x100, x1000) is shown in Figure 4.2. The dark output offset and its changes with lock-in amplifier gain setting must be known in order to determine the true signal measured with TOP2000. The increase in output offset with higher gain also limits the maximum detectable brightness for that gain setting.

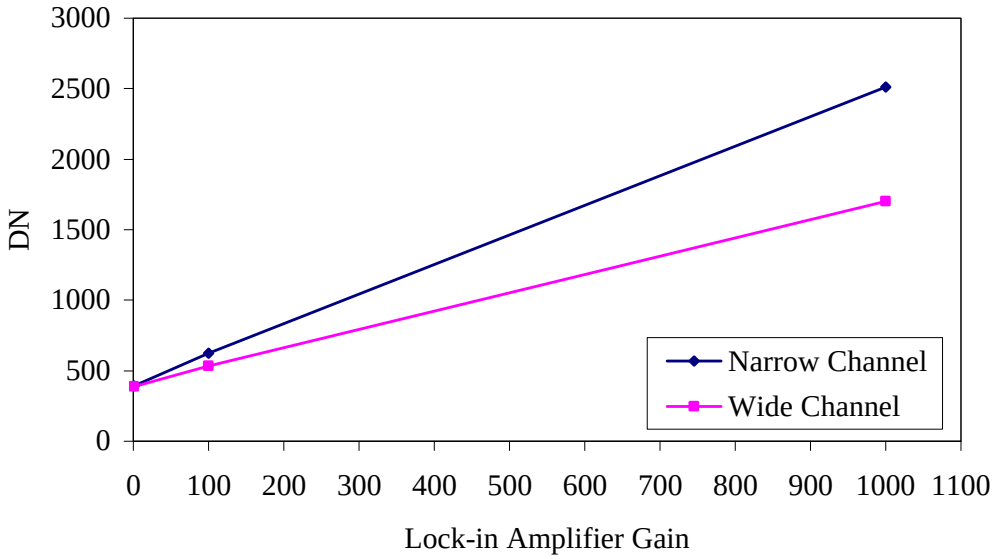

Figure 4.2: Dark output offset vs lock-in amplifier gain at room temperature.

4.2.4 Output Offset vs Temperature

During both testing and operation it was noticed that the dark output offset of TOP2000 fluctuated with changes in the ambient temperature. Originally it was planned to use a look-up table of the output offset for measured pre-amplifier temperatures to correct for changes in the offset. However, due to complications with the data set gathered during the Eureka, NU 2003 campaign (as described in Chapter 5) the table method proved inadequate and further tests to determine the TOP2000 sensitivity to temperature were conducted.

TOP2000 was operated in the dark at various ambient room temperatures to collect output offset DN vs pre-amplifier temperature sensor DN. The pre-amplifier temperature sensors were described in chapter 3 and the digital number (DN) is the digital conversion from the analog output voltage (V_{TEMP}). It is apparent from the results shown in Figure 4.3 that the output offset increases with increase in photometer temperature. The recorded temperature values, x-axis in DN, range from 12°C (1140 Temperature DN) to 27°C (1340 Temperature DN), see equation

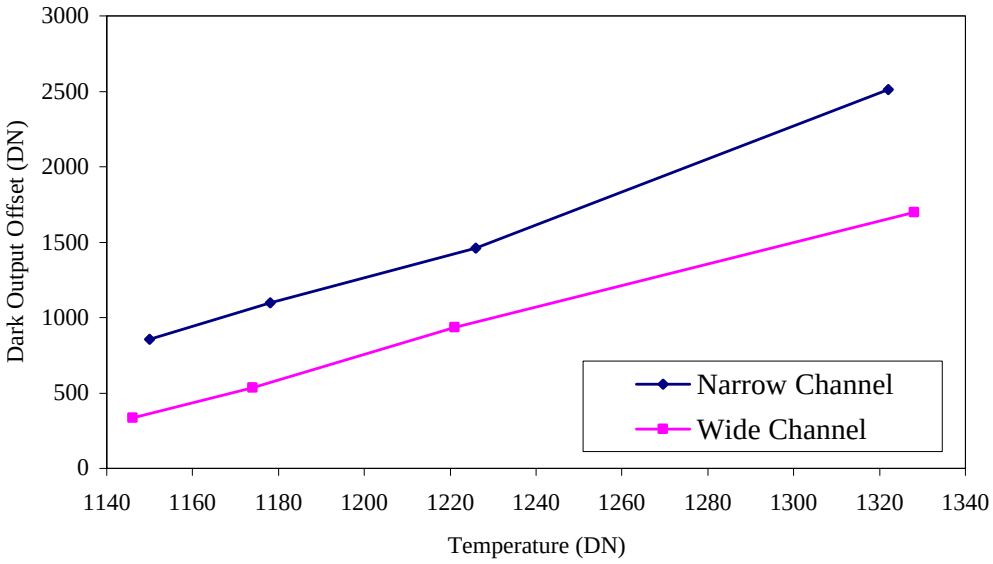

Figure 4.3: Output Offset vs Temperature at x10 x100 Gain

3.4. Theoretically the curve in Figure 4.3 should follow the pre-amplifier material dependent exponential dark current but for the range of measurements the DN change per °C is assumed linear. The slopes of a linear fit to the narrow and wide channel offset DN vs temperature, for an input gain of 10 and output gain of 100, are 126 DN per °C and 98 DN per °C respectively. Therefore it is apparent that the output offset of TOP2000 at high gain settings is very sensitive to ambient temperature fluctuations. This high temperature sensitivity proved to be a problem for TOP2000 operations in cold temperatures; this is discussed further in Chapter 5.

4.3 Output Offset Analysis

In this section theoretical explanations for the observed output offset characteristics are presented. Specifically given is an analysis of the noise generated throughout TOP2000 and its dependence on temperature.

4.3.1 Lock-in Amplifier and Noise

The signal recovery technique employed by the lock-in amplifier allows signals that are obscured by high levels of noise and interference to be measured [25]. The lock-in amplifiers used in TOP2000 at an output gain of 100 can detect signals in noise that is 100 times larger (dynamic reserve of 40dB). The large dynamic reserve allows weak signals to be detected during late twilight by TOP2000 but it does not eliminate all noise components from the photometer output.

The DC offset from the operational amplifiers in the pre-amplifier is removed by the demodulating circuit of the lock-in amplifiers. The demodulation process removes the major part of the out of phase noise from the output of the lock-in amplifier. However, there is still an in phase component of the noise spectrum from the pre-amplifier stage that reaches the output. As the reference waveform is a square wave, attenuated harmonic noise components also pass to the output of the lock-in amplifier. These noise components are demodulated and amplified according to the lock-in amplifier gain settings and so contribute to the output DN. The following describes how the in phase noise component at the input of the lock-in amplifier is passed to the output. The same analysis is valid at the harmonic frequencies but as they are attenuated (1/3 at the first harmonic) the fundamental frequency will be assumed the major noise source.

The analog input signal $v_{in}(t)$, see Figure 4.4, to the lock-in amplifier can be represented as [25]

$$v_{in}(t) = m(t)cos(\omega_o t) + n(t) \tag{4.1}$$

where m(t) is the amplitude of the sine wave at time t with a frequency ω_o and n(t) is the amplitude of band limited noise and can be defined as given in equation 4.2 [25].

$$n(t) = R(t)cos(\omega_o t + \phi(t)) \tag{4.2}$$

where R(t) and ϕ(t) are random changes of the amplitude and phase that are as-

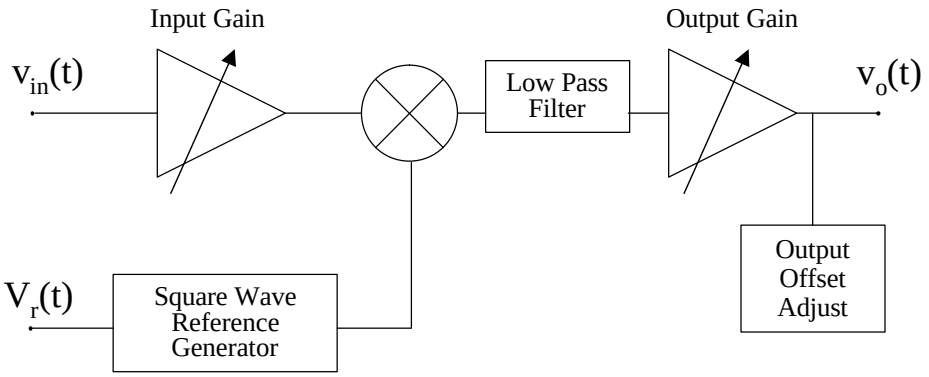

Figure 4.4: Noise analysis signal inputs and output for the lock-in amplifier.

sumed to vary slowly in comparison to $cos(\omega_o t)$. Expanding equation 4.2 gives

$$n(t) = R(t)cos(\phi(t))cos(\omega_o t) - R(t)sin(\phi(t))sin(\omega_o t) \tag{4.3}$$

and the in phase (n_i) and quadrature (n_q) noise can be defined as

$$n_i(t) = R(t)cos(\phi(t)) \tag{4.4}$$

$$n_q(t) = R(t)sin(\phi(t)) \tag{4.5}$$

Substitution of equations 4.2, 4.4 and 4.5 into equation 4.1 gives

$$v_{in}(t) = [m(t) + n_i(t)]cos(\omega_o t) - n_q(t)sin(\omega_o t) \tag{4.6}$$

If this input voltage, that includes both the signal and noise terms, is multiplied by the reference voltage (with a rms amplitude V_r) and passed through a low pass filter with a cutoff frequency less than $2\omega_o$ the output voltage is

$$v_o(t) = \frac{V_r}{\sqrt{2}}[m(t) + n_i(t)] \tag{4.7}$$

It is apparent from equation 4.7 that there is an in phase component of the input noise to the lock-in amplifier that is seen at the output. In other words the rms noise value from the pre-amplifier will be seen at the output of the lock-in amplifiers.

Another source of noise, actually a systematic error, from the lock-in amplifiers is the DC offsets of the internal operational amplifiers. As the output gain is increased the DC offset noise is amplified at the output and can not be removed by coupling, demodulating or filtering. The two noise sources (in phase pre-amplifier noise and lock-in amplifier output gain DC offset) both contribute to the increase in dark output offset with increasing gain as shown in Figure 4.2.

4.3.2 Pre-Amplifier Noise

The pre-amplifier noise is a combination of photodiode noise, resistor noise and op-amp noise. A DC offset voltage that is present at the output of the pre-amplifier results from the offset voltages of the operational amplifiers and the dark current from the photodiode. This DC offset is removed from the photometer output by the demodulating circuit in the lock-in amplifiers. However, as discussed there is a component of the random noise at the output of the pre-amplifier that affects the photometer output. This noise is mainly due to the photodiode dark current noise, the large feedback resistor thermal noise and the noise voltage of the pre-amplifiers.

The photodiode dark current under reverse bias conditions can be described by the diode equation given in equation 4.8 [24], where I_o is a material constant that is strongly dependent on temperature.

$$I_d = I_o(T)\left[\exp\left(\frac{-eV_r}{2k_BT}\right) - 1\right] \tag{4.8}$$

The temperature dependence in the exponential of the diode equation has little effect on the dark current It is the exponential temperature dependence of I_o, as shown in equation 4.9, that strongly affects the dark current with changes in temperature. The reverse bias dark current is mainly due to recombination of thermally generated electron hole pairs. As the temperature increases the EHP generation and the dark current of the photodiode increases.

$$I_o \propto \exp\left(\frac{-E_g}{k_B T}\right) \tag{4.9}$$

Noise due to random fluctuations of the number of discrete charges in the dark current is referred to as shot noise current and is described in equation 4.10 [24].

$$i_{n(dark)} = [2eI_d B]^{1/2} \tag{4.10}$$

This noise is not removed by the AC coupling of the lock-in amplifier and is therefore a component of the noise at the output of the photometer.

Similarly a component of the thermally generated noise from the resistors in the pre-amplifier will affect the photometer output offset. Each resistor in the pre-amplifier, see Figure 3.5, has a noise current that can be described by equation 4.11.

$$i_{nr} = \left[\frac{4k_B TB}{R}\right]^{1/2} \tag{4.11}$$

where k_B is the Boltzmann constant, T is temperature in Kelvin, B is the bandwidth and R is the value of the resistor. This noise current is temperature dependent and increases with increasing temperature.

The operational amplifier voltage noise also contributes to the total noise output of the pre-amplifier. The voltage noise comes from differences in the positive and negative inputs of the operational amplifier and is represented in data sheets as $V/\sqrt{Hz}$. The other noise sources of the pre-amplifier are orders of magnitude lower than the three mentioned above.

The total noise output of the pre-amplifier was calculated for different temperatures. At $22°C$ the calculated rms noise output is 0.883 mV. With the lock-in amplifiers at maximum gain (x1000) this would represent a noise output offset of approximately 720 DN. The calculated change in output offset DN from the temperature dependent preamplifier noise, at maximum gain, is 4 DN per °C. This calculated change in output offset DN per °C is much less than the measured change of 126

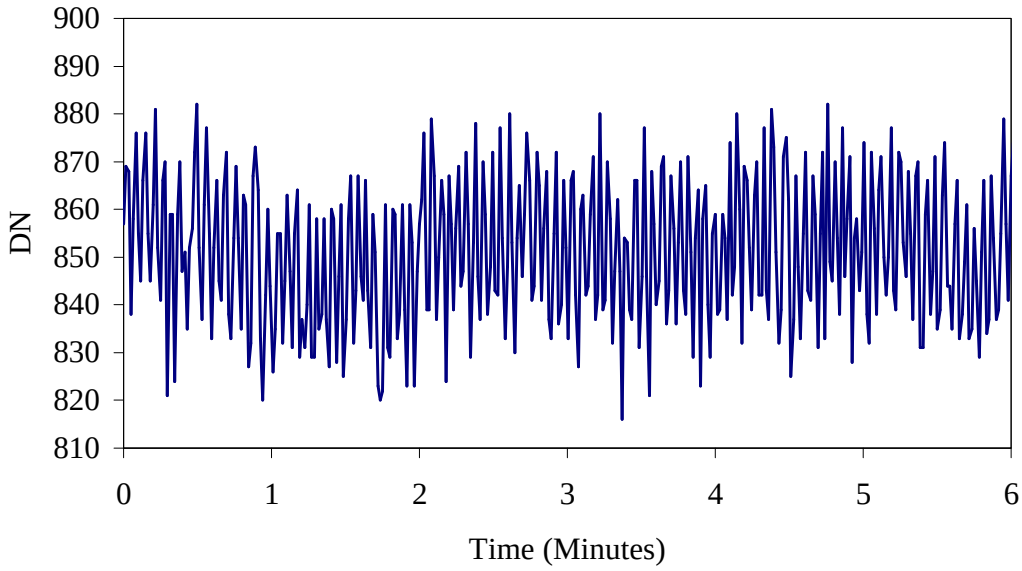

Figure 4.5: Narrow channel random noise of TOP2000 at maximum gain setting (x1000).

DN per °C and 98 DN per °C for the narrow and wide channels of TOP2000 and suggests that other effects must contribute.

4.4 TOP2000 Noise Performance

When the airglow brightness levels become low the measured brightness values, in DN, become comparable to the random noise measured by the analog to digital converter. The random noise signal fluctuates around the true output level (either in the dark or with signal input). Figure 4.5 shows the dark random noise for the narrow channel at maximum gain of TOP2000. These fluctuations were characterized for the three different gain settings of TOP2000 by using histograms to determine the standard deviation, in DN, about the mean.

The histograms for the three gain settings are shown in Figures 4.6 through 4.8. These histograms are for data collected with TOP2000 in dark conditions at room

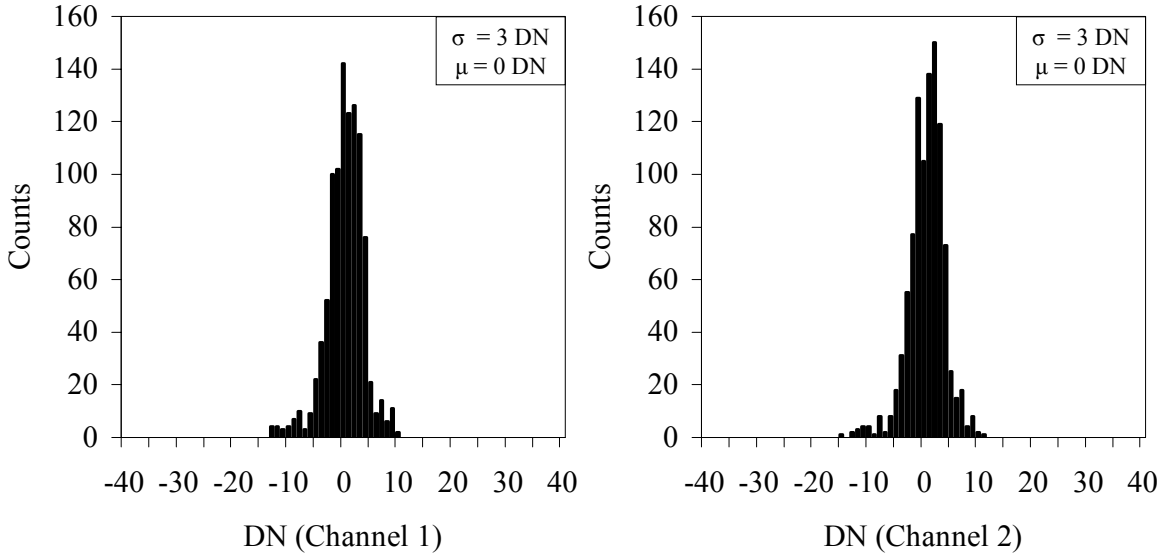

Figure 4.6: Noise Histogram for x1 input and x1 output gain setting. Channel 1 is the narrow channel and channel 2 is the wide channel.

temperature (approximately 26°) and represent the standard deviation (σ) in DN. The dark output offset average for each histogram has been removed to give a mean $\mu = 0$. Observations during testing suggest that the random noise about the mean of the output does not change significantly with temperature.

The calculated standard deviations for the low and mid gain settings are the same at 3 DN. However, at maximum gain the standard deviation increases to 12 DN for the narrow channel (channel 1) and 13 DN for the wide channel (channel 2). Therefore a difference of 24 DN must be present between the dark offset and detected signal level for reliable data in a simple measurement. Such low input brightness levels of the singlet delta emission only occur during late twilight and at night time.

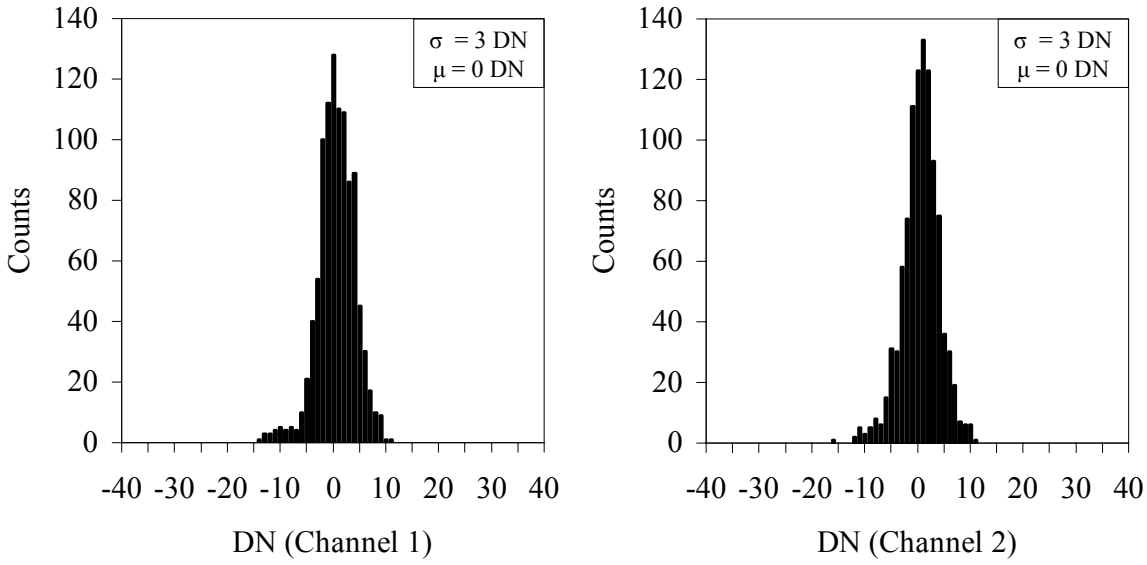

Figure 4.7: Noise Histogram for x10 input and x10 output gain setting. Channel 1 is the narrow channel and channel 2 is the wide channel.

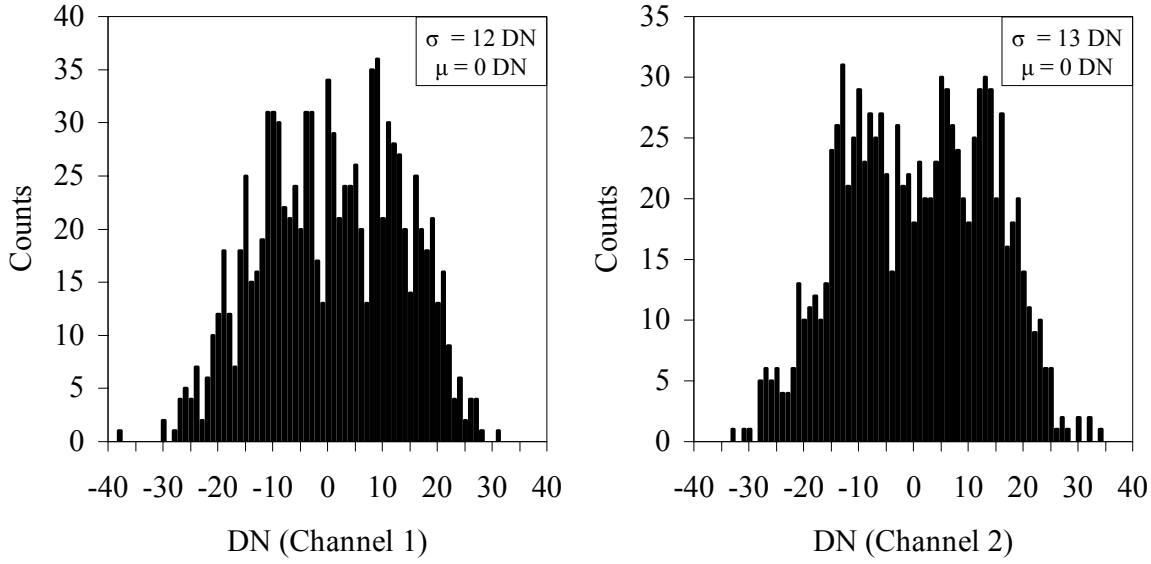

Figure 4.8: Noise Histogram for x10 input and x100 output gain setting. Channel 1 is the narrow channel and channel 2 is the wide channel.

4.5 Wavelength Calibration

The filter bandwidths for the narrow and wide channels and the beam splitter ratio were chosen in the original optical design so that the measured values for both channels would be the same for a flat spectrum input. The narrow and wide channel spectral response curves (which includes all filtering effects such as the pre-amplifier responsivity and filter shapes) were determined in order to test this ratio and to provide the necessary information for determining band capture fractions (fraction of the singlet delta band emission within the response curve and used to determine the height profiles and ozone concentrations from the measurements).

The spectral response of the TOP2000 photometer was determined using the ISAS scanning monochromator. The monochromator uses an input light source and outputs approximately a single wavelength of light. Initially the field of view was filled by a 50% transmission diffuser plate illuminated by an image of the ISAS scanning monochromator grating. Due to low brightness levels with a halogen lamp source (flat spectrum over the wavelength range of interest) a spectral response could only be determined for the narrow channel. The diffuser plate was removed and the TOP2000 photometer entrance aperature was placed as close to the monochromator exit slit as possible. The monochromator was stepped through the wavelength range 1130 to 1406nm at 2nm increments. The wavelength response for both the narrow and wide channels are shown in Figure 4.9. The narrow channel response without the diffuser plate grating image was comparable to the narrow channel response with the diffuser in place.

The areas under the narrow and wide channel response curves were calculated to determine the total filter shape ratio. The area of the narrow channel wavelength response curve is 1.8 times that of the wide channel. This differs from the theoretical ratio, which was designed to be 1, and is important for determining the singlet delta and ozone concentrations.

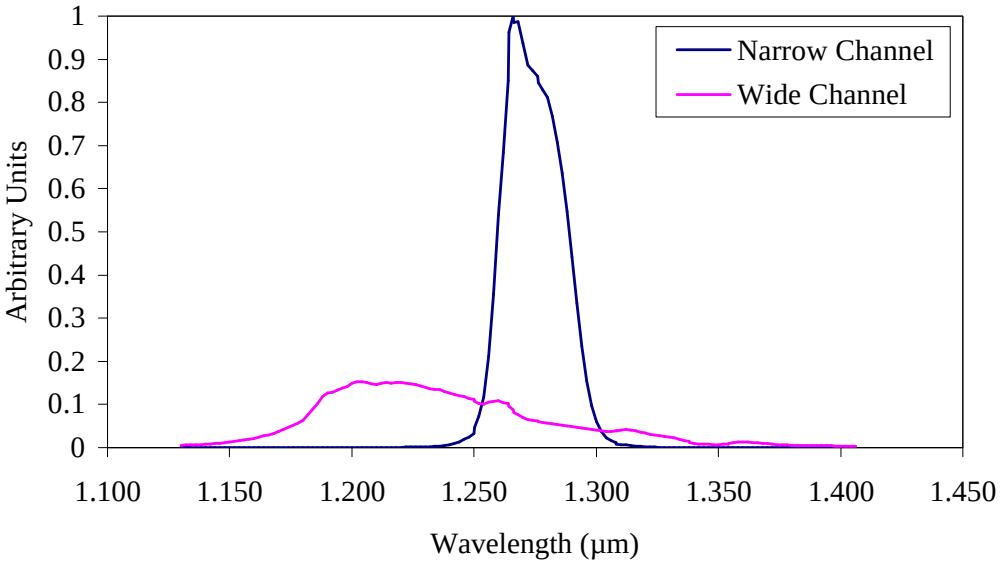

Figure 4.9: Narrow and Wide Channel Filter shapes.

4.6 Absolute Brightness Calibration

The absolute brightness calibration data for each channel of TOP2000 provides the conversion constant DN to brightness. These values are required in order to solve for the singlet delta and background continuum from the two equation, two unkowns dual channel photometer method described in Chapter 2. The absolute brightness calibration requires both the input brightness and its spectrum to the photometer to be known.

The absolute brightness calibration was done using the ISAS black body radiation source which provides a known spectrum and brightness output for a set temperature based on the Planck function. A diagram of the laboratory setup is shown in Figure 4.10. The radius (r) was such that the brightness across the diffuser plate from the source aperature could be considered constant. The brightness at TOP2000 from the black body radiation source is given by:

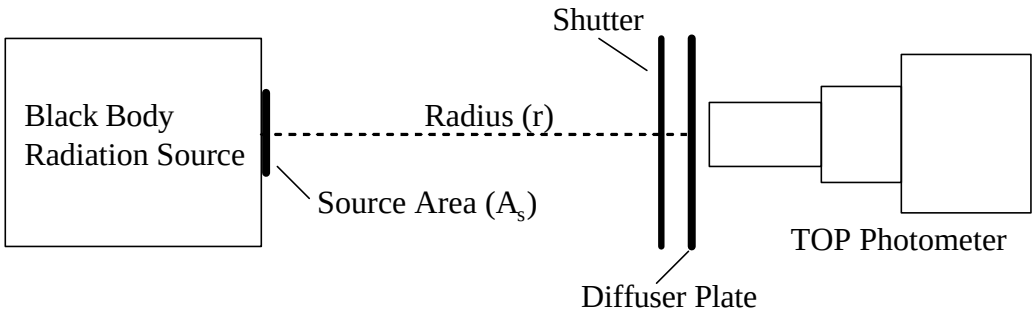

Figure 4.10: Absolute Brightness Measurements Setup

$$B_d = B_{bb}\left[\frac{photons}{s\ cm^2\ ster\ nm}\right]\ 2\pi\,[ster]\ \ A_s\left[cm^2\right]\ \ \frac{1}{2\pi r^2\,[cm^2]}\ \frac{1}{2}\ \frac{1}{2\pi\,[ster]} \tag{4.12}$$

where B_{bb} is the brightness from the black body radiation source, $2\pi[ster]$ is the half a sphere field of view for the emitted photons from the black body source with a total area of $A_s[cm^2]$. The photons from the source area are uniformly dispersed over the half sphere ($2\pi r^2$), which increases with radius r. The diffuser plate is 50% transmission and 50% reflection so only half the incoming photons enter TOP2000. On the photometer side of the diffuser plate the photons again spread over a half sphere field of view $\frac{1}{2\pi[ster]}$. Therefore, the brightness at TOP2000 can be written as:

$$B_d = B_{bb}\frac{A_s}{4\pi r^2}\ \ \left[\frac{photons}{s\ cm^2\ ster\ nm}\right] \tag{4.13}$$

The brightness of the black body radiation source as measured by TOP2000 is given by:

$$DN = \sigma \int B_{bb}(\lambda)\frac{A_s}{4\pi r^2} f_n(\lambda) d\lambda\ A_d\omega_d \tag{4.14}$$

where σ is the conversion constant from photons per second to DN, the integral of B_{bb} and f_n, the normalized channel filter shape, is the band capture fraction and

$A_d\omega_d$ is the area and field of view of the detector. As the analysis to calculate the signal brightness from DN uses the same filter shape, the multiplication constant for the normalized filter is included in the conversion constant σ. The absolute brightness constant, k, then includes σ and $A_d\omega_d$ into the single calibration term that is calculated from the absolute brightness calibration data.

The black body source brightness in $J/s/m^2/m$ is the Planck function given in equation 4.15.

$$B_{bb} = \frac{2\pi hc^2}{\lambda^5 \left[e^{\frac{hc}{\lambda k_B T}} - 1 \right]} \left[\frac{J/s}{m^2 m} \right] \tag{4.15}$$

where λ is the wavelength, h is Planck's constant, c is the speed of light, k_B is Boltzmann's constant and T is the temperature in Kelvin. The units of Joules can be converted to photons by dividing by the energy per photon (hc/λ).

In order to determine an accurate absolute brightness calibration constant and to verify that the photometer response is linear to linear changes in brightness the black body source was run at several different temperatures at each of the three main gain settings. The absolute calibration constants can be determined from equation 4.14 for different black body brightnesses. Figure 4.11 is an example of the measured output, in DN, for different input brightness for an input gain of x10 and an output gain of x100. These results demonstrate TOP2000's linear response to changes in input brightness. Each data point corresponds to a different temperature setting of the black body radiation source. The equation for both linear trendlines are shown and the values of the slopes are the k_N and k_W calibration constants for the narrow and wide channels respectively. The absolute brightness calibration constants for both channels, at each gain setting, are summarized in Table 4.1 where k_N and k_W are the narrow and wide channel calibration constants with units of DN per photon/s/cm^2/ster.

Table 4.1: Narrow and Wide Channel Absolute Brightness Calibration Constants

Gain	k_N (Narrow Channel) [DN/photon/s/cm^2/ster]	k_W (Wide Channel) [DN/photon/s/cm^2/ster]
x1 x1	6.75e-12	2.73e-12
x10 x10	7.43e-10	3.00e-10
x10 x100	6.90e-9	2.78e-9

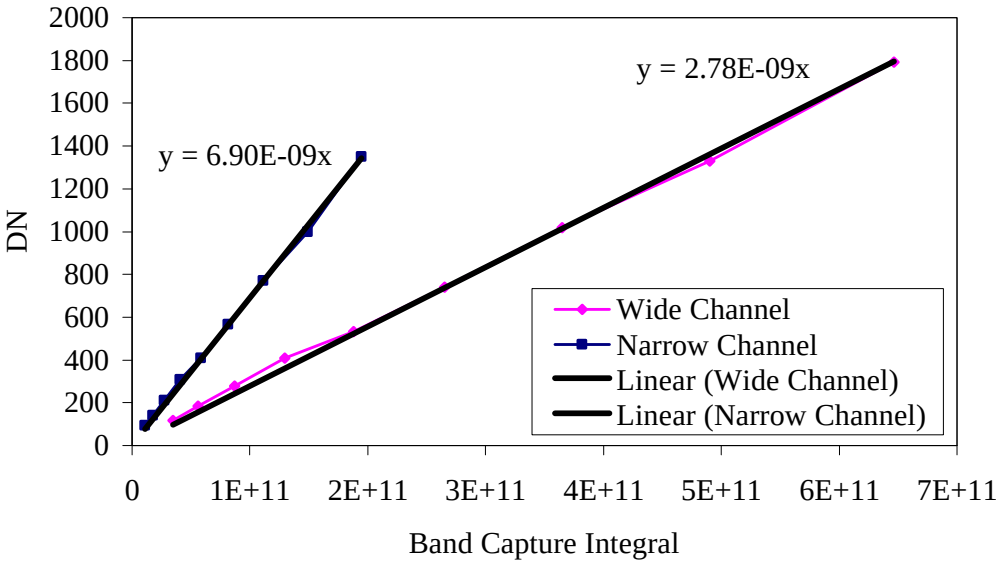

Figure 4.11: Absolute brightness calibration curves that yield k_N and k_W.

4.7 Summary

The characteristics of the output offset were described and related to certain aspects of the photometer circuitry. Specifically changes in output offset with different lock-in amplifier settings and operating temperatures were detailed. A simple analysis to provide some insight into the characteristics of the offset was given. The large sensitivity of TOP2000 could not be satisfactorily explained through the noise analysis and requires further investigation. The noise performance of TOP2000 was demonstrated. The wavelength calibration and absolute brightness calibration procedures were described together with the calibration results.

Chapter 5

Experimental Observations

5.1 Introduction

This chapter shows the progression of observations and the modifications made in an attempt to improve the quality of data from TOP2000. Data observations from Saskatoon, SK and both the fall 2003, spring 2004 data collection campaigns in Eureka, NU are given. It is also demonstrated that the shutter system was able to remove the temperature dependent fluctuations in the processed data. Finally the twilight signal decay in both the narrow and wide channels is presented to demonstrate the measurement of the background scattered light and singlet delta emission brightnesses.

5.2 Saskatoon

Prior to making twilight measurements TOP2000 was operated in the ISAS optics laboratory. Using an incandescent bulb as the light source TOP2000's functionality was tested to verify the computer control of the lock-in amplifier settings, the data collection and storage by the computer. During this laboratory testing it was noticed that the output offset at high gains was sensitive to room temperature. Initially it

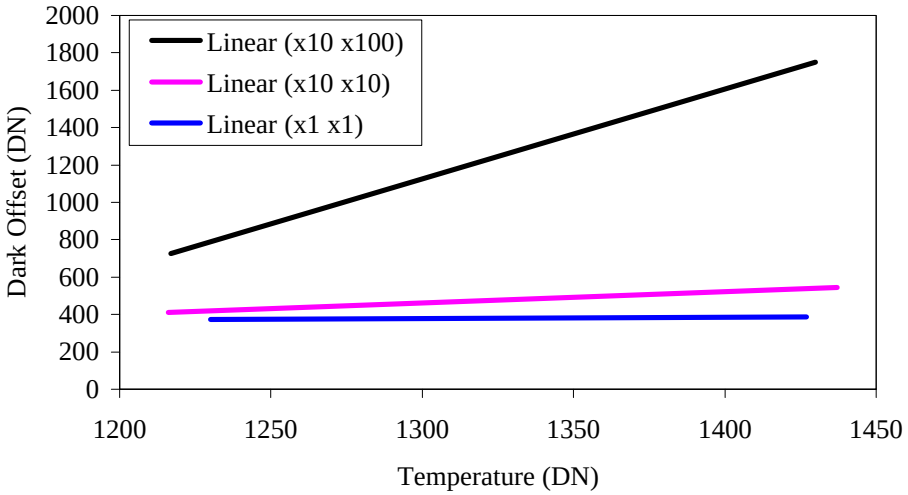

Figure 5.1: TOP2000 dark offset vs temperature data measured for the narrow channel in the laboratory.

was planned to remove the temperature dependent offset from the measured signal using the measured dark output offset vs. temperature characteristics. The linear trendlines based on the measured dark offset vs temperature during operation in the lab, for three different gain settings of the narrow channel, are shown in Figure 5.1. It will be shown later that the look-up table method based on this dark offset vs temperature data to remove the temperature dependent offset was inadequate.

Once the required changes were complete for proper operation of TOP2000 in the laboratory the instrument was moved to a hatch in the roof of the Physics Building of the University of Saskatchewan to make the first twilight observations. These observations demonstrated the TOP2000 ability to measure the singlet delta twilight signal. Figure 5.2 shows the narrow channel signal for late twilight conditions (at time 0 the sun has set to 8 degrees below the horizon). The operating temperature of TOP2000 while making these was stable at approximately room temperature.

The airglow and laboratory measurements collected in Saskatoon, SK prior to the

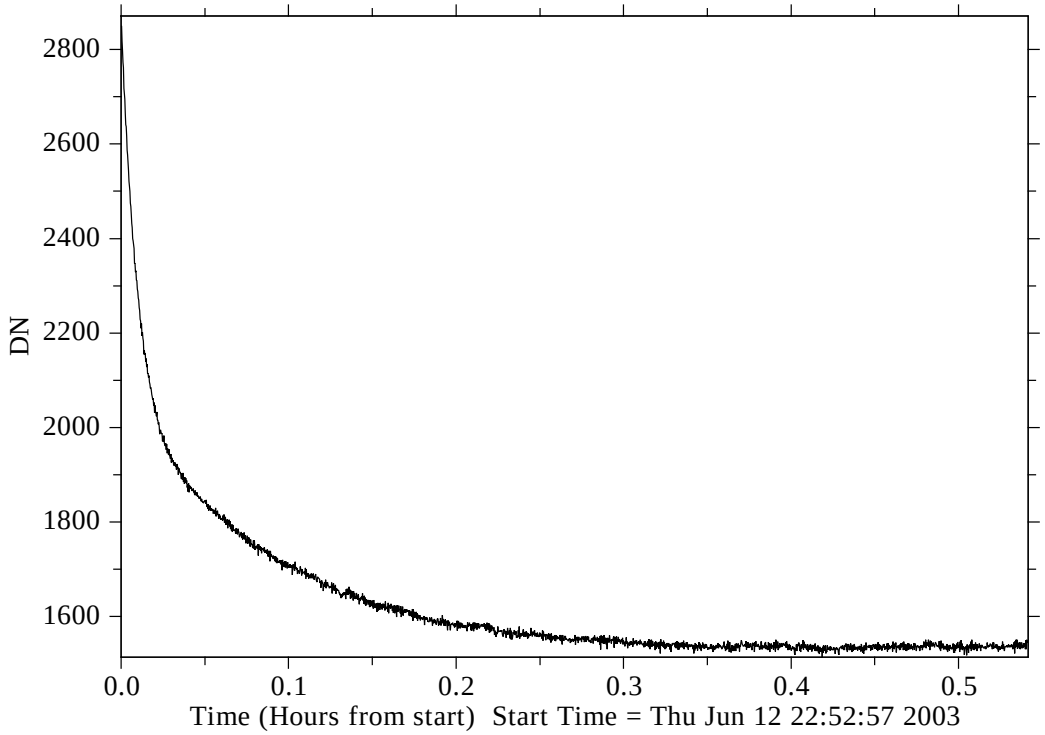

Figure 5.2: Narrow channel signal decay, Saskatoon June 12, 2003

Eureka, NU campaigns demonstrated that the designed and constructed two channel photometer TOP2000 was ready for operation. Also, the operation procedures and fixes to many of the problems that could arise while in the north were determined during the Saskatoon measurements.

5.3 Eureka 2003

During the fall of 2003 observations with TOP2000 were made at Eureka, Nunavut over a six week period as the sun was dropping lower into polar winter darkness. Eureka, NU, is an isolated weather station located at 80° N and 86° W. The station is operated by Environment Canada with transportation in and out approximately once every three weeks by airplane during the non summer months. For operation in an isolated environment both TOP2000 and several pieces of test and repair equipment were shipped to the weather station.

TOP2000 was setup in the environmental box which was placed outside close to the building that housed the computer for communication, control and data storage. The outside exposed power and communication cables that were run to TOP2000 from within the building were covered with snow and dirt to prevent cable breakage in the cold weather and strong winds. During operation the outside temperatures at Eureka ranged from approximately -15 to -35 degrees Celsius with periodically strong winds. The thermostat controller turned on and off a 150 Watt strip heater within the environmental box. Initially the thermostat controller temperature was set too low for proper operation of TOP2000. In an attempt to minimize thermally generated noise the environmental box temperature was set to approximately 10°C. During cold and windy weather the 10 degree temperature setting proved inadequate to maintain a constant temperature within the box. The thermostat control was raised up to 20°C and remained at that setting for the remainder of the campaign. With this suitable thermostat temperature setting TOP2000 ran continuously for several weeks at a time with a few periods of shutdown due to severe weather and

intermittent checks on the condition of the instrument.

The region in and around Eureka, NU, is considered to be a desert. The air is very dry and static electricity builds up and discharges very easily. Great care was therefore taken to prevent static discharge through the instrument electronics. The high arctic weather conditions can also be rather challenging with high winds blowing a fine mixture of dirt and snow. During both campaigns the environmental box was tied down to prevent the instrument from being blown over in high winds and data collection from TOP2000 was stopped during the more severe storms.

An example of the twilight decay of singlet delta with clear sky conditions measured at Eureka in the fall of 2003 by TOP2000 is given in Figure 5.3 (the start of the plot at hour 10 is approximately 7:30pm local time). Unfortunately due to the coarse on and off nature of the strip heater the operating temperature within the environmental box fluctuated and caused a ripple in the data. This temperature dependent ripple results from the sensitivity of the dark output offset to changes in the operating temperature of TOP2000, see Chapter 4. An attempt to minimize the ripple by changing the air flow setup within the box proved ineffective. As the heater in the box increased the operating temperature the dark output offset increased, as the box cooled the offset decreased. The period of the offset ripple varied according to the outside weather conditions (a shorter period for colder outside temperatures) and the ripple was out of phase with the measured pre-amplifier temperature. During regular operation it was found that if the weather conditions changed such that the heater on and off cycle changed the period of the temperature dependent ripple also changed. The non-periodic pattern in the offset ripple therefore made the data analysis difficult. The ripple could not be removed with the look-up table as its fluctuations were based on the outside temperature rather than the pre-amplifier temperature.

While the Eureka 2003 measurement campaign was a success in terms of the operation of TOP2000 the data collected is difficult to use due to the temperature dependent ripple. Upon completion of this campaign and return to Saskatoon,

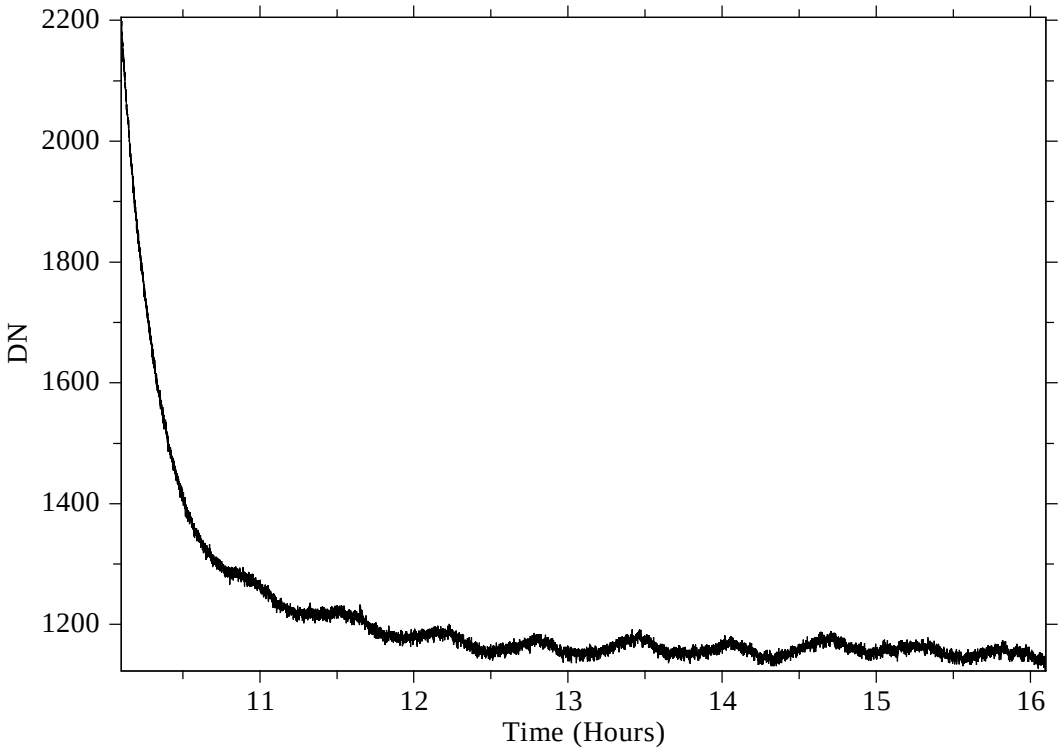

Figure 5.3: Eureka, NU October 10, 2003 narrow channel signal decay demonstrating temperature dependent ripple.

modifications were made to the instrument setup to minimize the temperature dependent fluctuations of the dark output offset. This necessitated an improvement in the heating control. A shutter system was also added to permit removal of the variations in the dark output offset and allow useful scientific data collection during the next Eureka campaign in 2004.

5.4 TOP2000 Modifications

No changes were made to the instrument itself after the first operation in Eureka, NU. However, in order to address the temperature dependent ripple problem two modifications were made to the environmental housing box. First improved temperature control was required so a commercial PID (proportional integral derivative) temperature controller was installed. The thermocouple (temperature sensor) was placed inside TOP2000 and a blanket heater was wrapped around the instrument. The PID controller set temperature could be adjusted through the serial port communication allowing for temperature adjustment without requiring the environmental box to be re-opened. The coarse thermostat controller was retained to help maintain the ambient temperature of the box. The heater wrapped around TOP2000 was set a few degrees higher then the thermostat control temperature to ensure that the instrument was maintained at a constant temperature above the ripple effect of the coarse thermostat. Unfortunately this heater arrangement was not optimum and the temperature dependent ripple was still present in the data collected during the second Eureka campaign in 2004.

Even though a temperature dependent ripple was still present in the 2004 Eureka data the installation of a shutter system permitted removal of this effect. As the dark output offset vs temperature data look-up table could not be used to remove the offset from the data measurements periodic dark output offset measurements were included in the operation of TOP2000. The shutter system was designed to prevent light that entered the window of the environmental box from reaching the

entrance aperture of the photometer. A control box that could be adjusted to set the open and closed time of the shutter was situated inside the operation building and control to the shutter motor was via a cable to the environmental housing box. The shutter and the shutter control box are shown in Figure 5.4. When power is applied the shutter defaults to turning and when the shutter passes one of the positioning switches the control box is triggered to shut the motor off for a given period based on the time constant selected on the control box. A green LED on the control box indicates the shutter position (both LEDs off means the shutter is rotating).

With the inclusion of the shutter the dark output offset with its variations in time (mainly dependent on temperature) could be removed from the measurements. By making shutter open and closed measurements at a faster rate than the fluctuations in the dark output offset and the emission decay of interest the required signals are generated. A detected light signal that includes the dark output offset and the airglow brightness is measured while the shutter is open. While the shutter is closed only the dark output offset signal is measured.

5.5 Eureka 2004

Singlet delta observations were made with the modified setup of TOP2000 during spring 2004 at Eureka over a nine week period as the sun was rising toward polar summer conditions (24 hour sunlight). The outside temperature over the nine week campaign averaged near -40 degrees Celsius. As previously mentioned it was noticed that the new heater and controller configuration within the environmental box did not improve the temperature dependent ripple in the data. However, due to the weather conditions the instrument was not moved inside in an attempt to improve the heater arrangement and temperature control. Both the developed shutter system and TOP2000 ran for approximately eight and a half weeks continuously (no data collection during severe storms).

The measurements obtained with the shutter opening and closing during the

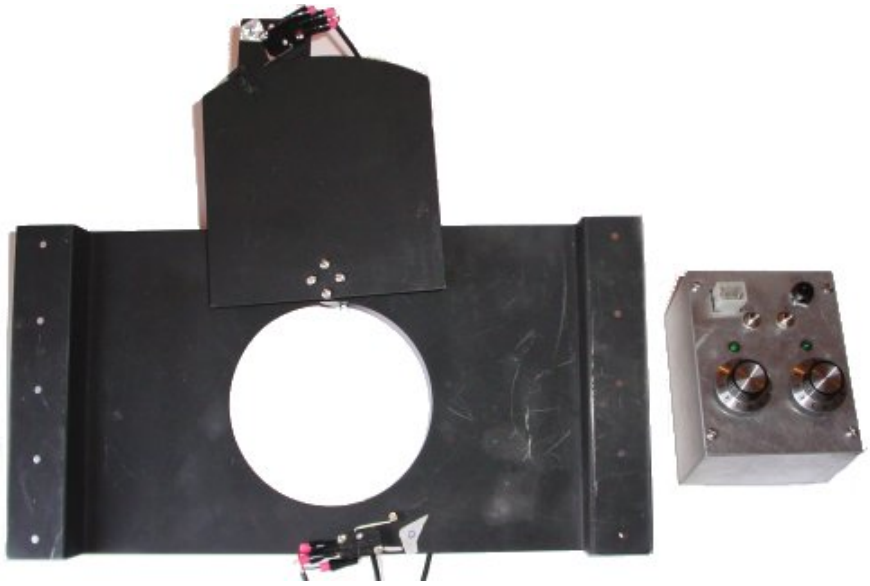

Figure 5.4: TOP2000 shutter and control box designed to work with the environmental box.

day and twilight for a clear sky (no clouds) is shown in Figure 5.5. For these narrow channel measurements at Eureka on March 9, 2004 both the shutter and PID temperature controller modifications were in place (local time at hour 0 is 4:14pm). The signal change at 3.5 hours is due to a gain setting change of TOP2000. The lower gain setting data (0 to 3.5 hours) has been multiplied to represent the true brightness of the airglow. The temperature dependent ripple is not evident in Figure 5.5 although it is still present and becomes important in the later twilight hours. This will be demonstrated in the data processing section. However, the dark output offset data collected during the shutter closed periods throughout the decay does provide a method to remove the temperature dependent fluctuations in the measurements.

During the course of both Eureka campaigns the sky conditions experienced ranged from clear skies to full cloud cover. Good measurements with clear skies were logged when there was approximately 5 percent or less cloud cover (based on

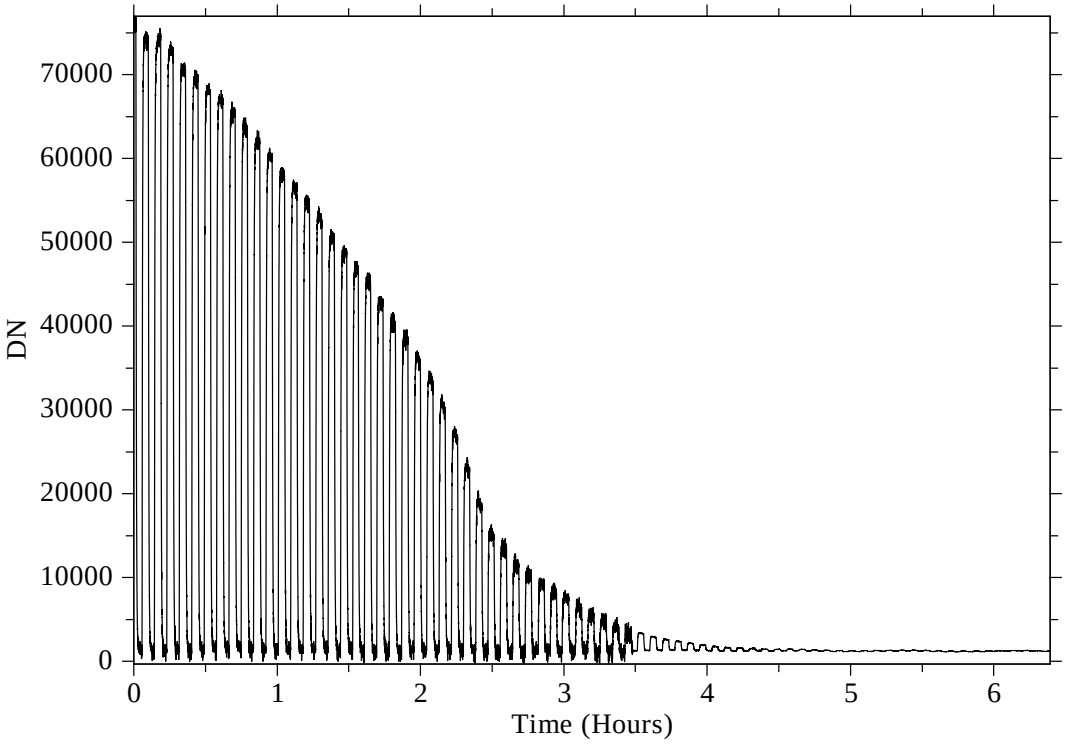

Figure 5.5: Eureka, NU narrow channel signal decay for March 9, 2004 with both PID temperature control and shutter system (no clouds).

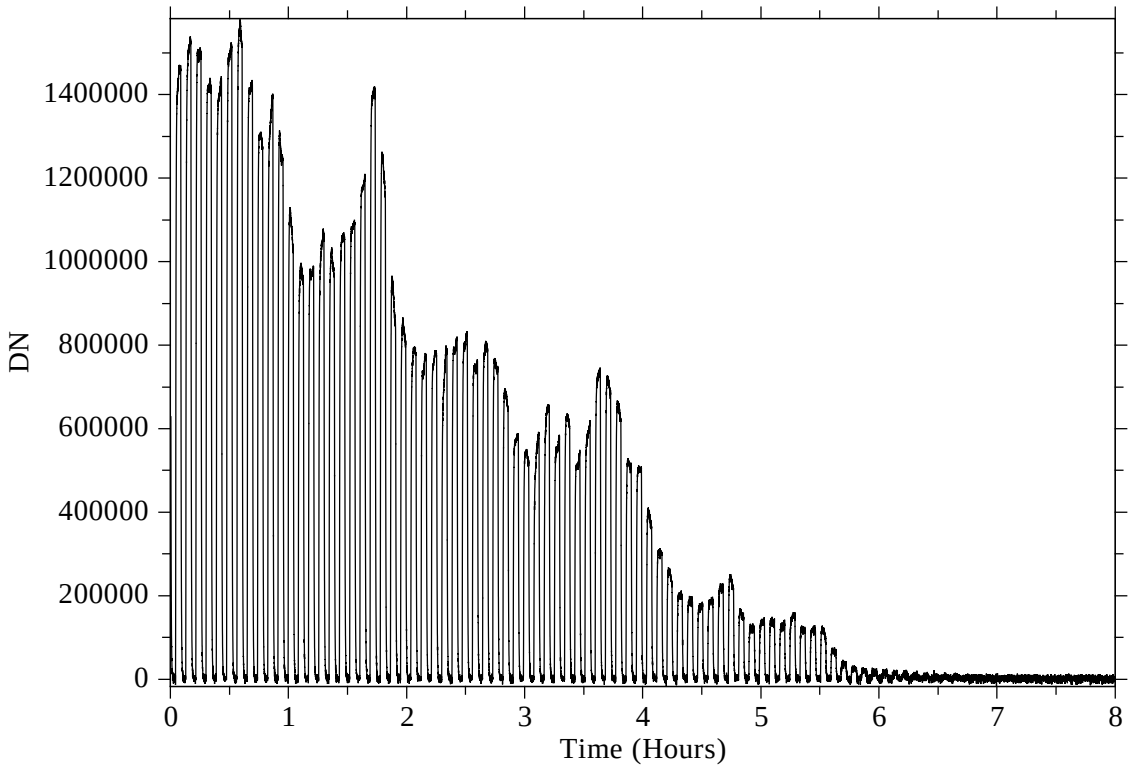

Figure 5.6: Eureka, NU narrow channel signal decay for the cloudy day of March 21, 2004.

visual observations) and no clouds in line with the setting sun. Measurements made in the presence of cloud cover are evident in the collected data due to the increased broad-band scattered light from over head clouds. The late twilight and evening sky conditions were logged according to Environment Canada's cloud cover records and visual observations of stars. An example of measurements made with TOP2000 with overhead cloud cover is shown in Figure 5.6. The data is from the narrow channel at the lowest gain setting (x1 input, x1 output) and the signal varies, along with the twilight decay, as the brightness of the scattered light from the overhead clouds varies.

5.6 Processed Data

In order to process the data Python scripts were written to load, manipulate and plot the data collected by TOP2000. To permit analysis of the measured airglow twilight decay the set of data files for a given day, each containing approximately 2 hours of observations, were placed in a processing directory. The Python scripts then loaded each file concatenating them in time and multiplying the DN of lower gain settings if required. In this way a DN vs time plot could be generated, Figures 5.3 and 5.5 are examples of these plots.

The Eureka 2003 measurements were not analyzed due to the difficulty in removing the temperature dependent ripple. However, for the Eureka 2004 measurements the dark output offset was removed using the shutter closed information. This provided data points that represent the atmospheric emission brightnesses in the narrow and wide channels with the temperature effects removed.

The data analysis procedure can be demonstrated using the March 9, 2004 data shown in Figure 5.5. The signal level just after the shutter opened, or closed, required a settling time to allow for the 10 second time constant associated with the low pass filter in the lock-in amplifiers. Therefore, the 30 seconds of data (3 times the filter time constant) following the shutter open or closed operation were removed. The valid data for the dark and signal data sets that remained were then averaged for a single value. The dark data were linearly interpolated to get dark values at the times corresponding to the signal data points. The processed signal and dark data values for March 9, 2004 are shown in Figure 5.7 (these are the separated shutter open and shutter closed signals shown in Figure 5.5). The decaying data points (starting at approximately 75000 DN) are the averaged values of the measured signal brightness while the shutter was open for the narrow band channel of TOP2000. The lower data points, just above zero, are the averaged dark values from the shutter closed sections linearly interpolated to the same time as the signal data points. Figure 5.8 is a zoomed version of Figure 5.7 and demonstrates the temperature dependent

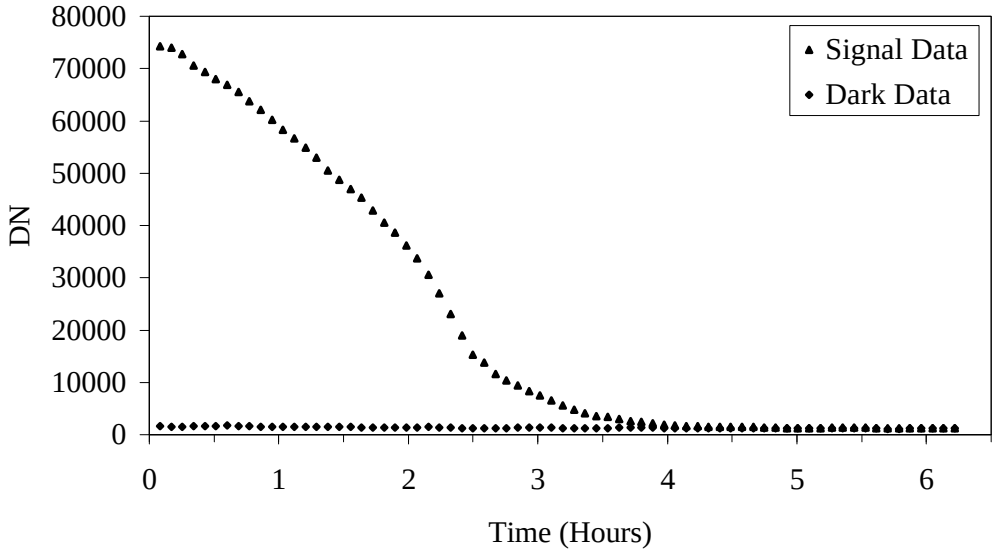

Figure 5.7: Averaged narrow channel signal and dark data from Figure 5.5 for Eureka, NU, on March 9, 2004

ripple that is present in both the signal and dark data as described in section 5.5.

The dark output offset data points are subtracted from the signal data points. The calculated DN after the subtraction is proportional to the input brightness with the temperature effects of the offset removed. The processed data from both channels on March 9, 2004 is shown in Figure 5.9 with a zoomed in version in Figure 5.10. The processed data may still contain small errors from the linear interpolation of the averaged values method used. These errors may need to be corrected in the late twilight, evening measurements when determining singlet delta concentrations using the absolute brightness calibration data. The analysis to determine singlet delta concentrations using the absolute calibration requires the solution to the integrals given in equations 2.8 and 2.9. In order to calculate these integrals knowledge of the singlet delta and background spectra at each altitude and the transmission of each to the ground is required. This calculation is beyond the scope of the thesis. However, the small errors in the processed data do not preclude the determination

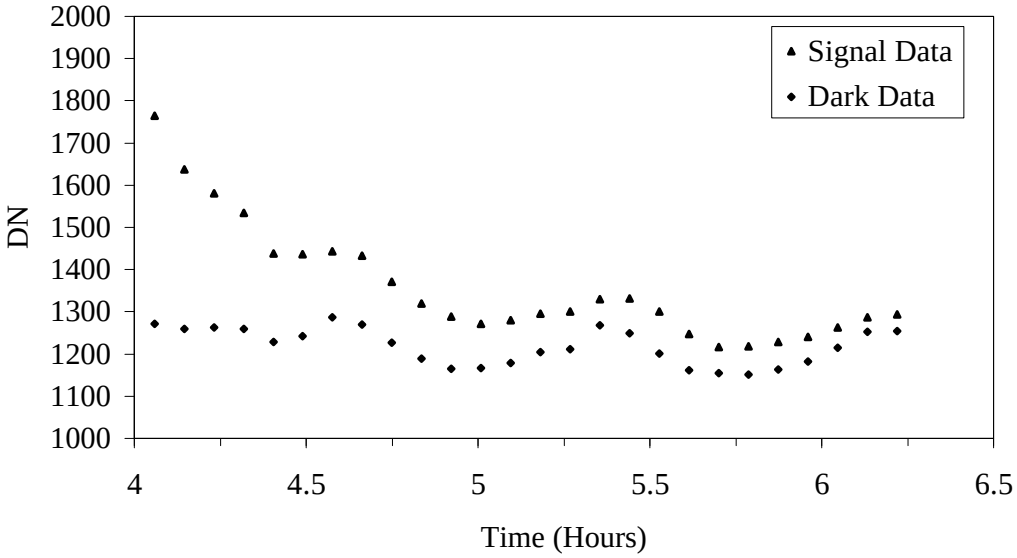

Figure 5.8: Zoomed narrow channel data for Eureka, NU March 9, 2004

of the decay rates of singlet delta at different times as the decay curve can still be determined.

As mentioned the processed data can be used to determine both singlet delta and background signal levels using the absolute calibration data. As described in Chapter 2 ozone concentrations can be derived from these signals. The ability to derive singlet delta decay times at different altitudes from the data collected by TOP2000 was also discussed in Chapter 2. Once the production of singlet delta from the sun has stopped and the scattered light at 1.27 microns is no longer entering the instrument the detected signal is from primarily singlet delta emission decay.

It is apparent from Figure 5.9 that the background signal measured by the wide band channel (channel 2) is larger than the narrow band channel (channel 1) signal during the day. As the sun sets the source of the background signal decreases faster than the emission from the singlet delta. As shown in Figure 5.10 the wide channel and narrow channel data eventually exhibit the same changes in input brightness. At this point (starting at 4.5 hours) the narrow channel and wide channel are both

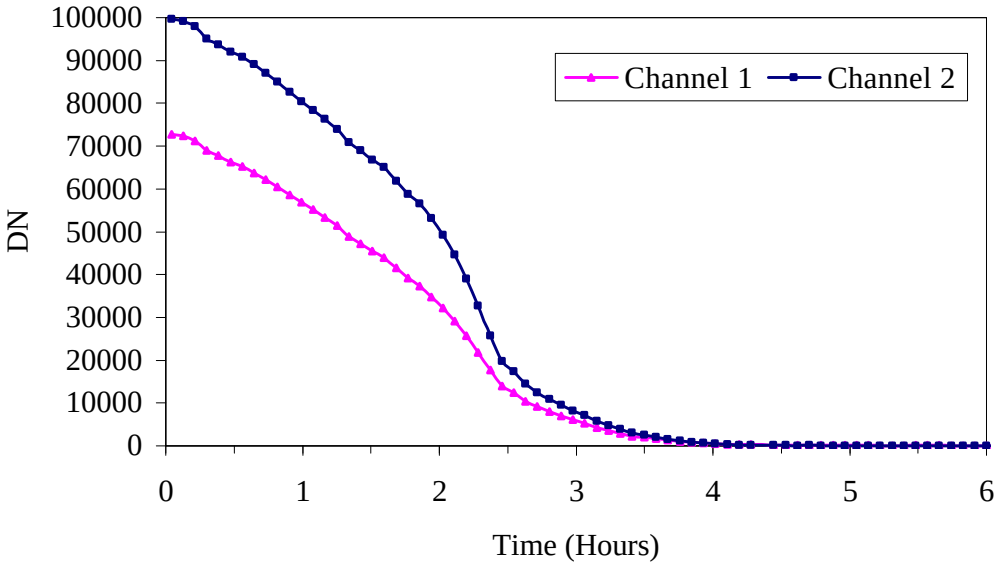

Figure 5.9: Both Channels Data for Eureka, NU March 9, 2004

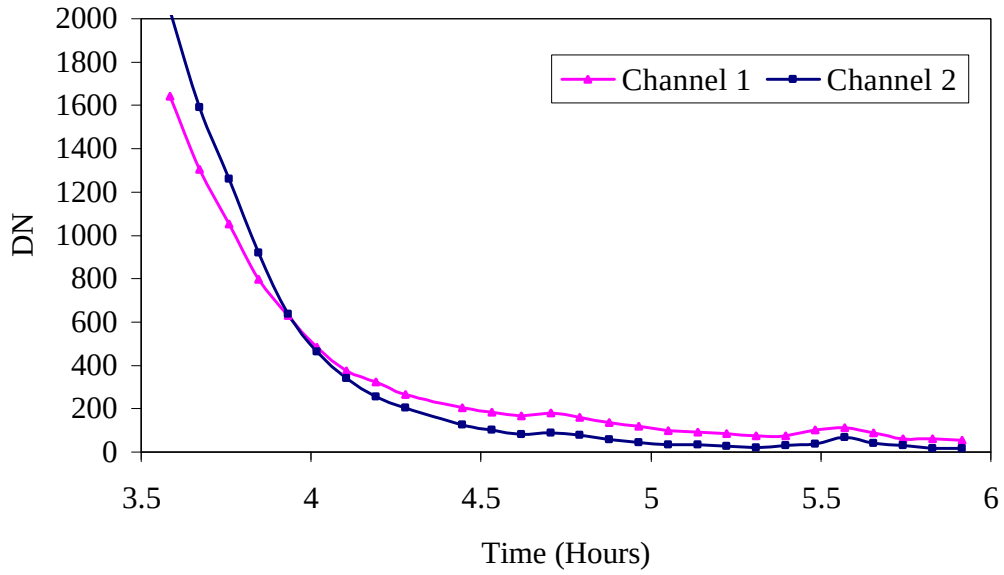

Figure 5.10: Both Channels Data Zoomed for Eureka, NU March 9, 2004

predominantly measuring the singlet delta emission decay. The singlet delta emission spectrum only fills a percentage of the wide channel spectral response and therefore its signal is an attenuated value with respect to the narrow channel signal. The increase in signal in Figure 5.10 between 4.5 and 5 hours and again just past 5.5 hours are a result of the linear interpolation technique. Similar errors occur before these times but are insignificant compared to the signal values. The error becomes important only in late twilight and nighttime measurements and could be reduced if a more accurate interpolation technique was applied.

5.7 Summary

The initial observations of TOP2000 from Saskatoon were described. The observations from both Eureka, NU campaigns were shown together with the modifications made to improve the scientific value of the data. Some of the difficulties with instrument operation in the high arctic were described. The temperature dependent ripple that was evident in the fall Eureka data was described and a method for removing it with the use of shutter data was shown in the spring Eureka data. The method of processing the data and an example of the results were also presented.

Chapter 6

Data Analysis

6.1 Introduction

Singlet delta altitude profiles during the twilight decay are presented from measurements made with the InfraRed Imaging System (IRIS) on the Odin satellite to demonstrate the validity of the assumptions made in Chapter 2. The steps involved in calculating the singlet delta decay times from the narrow channel measurements made by TOP2000 are outlined. The scientific value of TOP2000 is demonstrated by analyzing singlet delta decay times from data collected in Eureka, 2004. Further comparison and validation of TOP2000 is made by presenting measurements made in Saskatoon, 2004 by TOP2000 and comparing them with the Eureka, NU 2004 measurements.

6.2 Singlet Delta Decay Measured by IRIS

The validity of the assumption that the measured decay rates of singlet delta from the ground are heavily weighted towards the peak emission altitude is demonstrated by the singlet delta decay profiles measured by the IRIS instrument around the equator.

The singlet delta altitude profile decay measured by the IRIS instrument on the Odin satellite is shown in Figure 6.1. These data are made up from longitudinally averaged measurements for each time after sunset at the equator. The longitude average data is calculated from each time the satellite measures the singlet delta emission at a given time after sunset over the course of several orbits at different longitudes around the equator. By combining these measurements the altitude profile time sequence of the decaying singlet delta emission during twilight is obtained. Sample vertical cross sections at different times during the twilight singlet delta decay are shown in Figure 2.5. At time zero the sun has just set below the horizon. As the sun drops further below the horizon the shadow height increases and the singlet delta emission at the lower altitudes begins to decay. The majority of the singlet delta between 50 and 65 kilometers decays quickly, the emission between these altitudes has a lower brightness value than the higher altitude emission after 35 minutes (see Figure 2.5 from Chapter 2). The excited state molecular oxygen at higher altitudes (75 to 100 kilometers) has a lower collision frequency with the quenching molecules and therefore decays at a rate that is closer to the radiative decay time (slower than the lower altitudes). Figure 6.1 also shows that the majority of the change in the total column brightness (sum of the vertical volume emission rates at a given time) of the singlet delta emission is due to the lower altitude singlet delta emission decaying away faster than the higher altitudes. It is also apparent that this decay altitude increases with time. The brightness decay for three different altitudes from the altitude profile singlet delta emissions shown in Figure 6.1 is given in Figure 6.2 and demonstrates the faster decay rates of the lower altitude singlet delta a little more clearly.

The calculated decay times for the singlet delta emission at 57 and 70 kilometers shown in Figure 6.2, measured by IRIS, are shown in Figure 6.3. At time equal 20 minutes, the x-axis of Figure 6.3, the sun is 5 degrees below the horizon (at the equator). As explained earlier the lower altitude singlet delta decays faster than the upper altitude singlet delta. Therefore the decay time when the sun is at 5 degrees

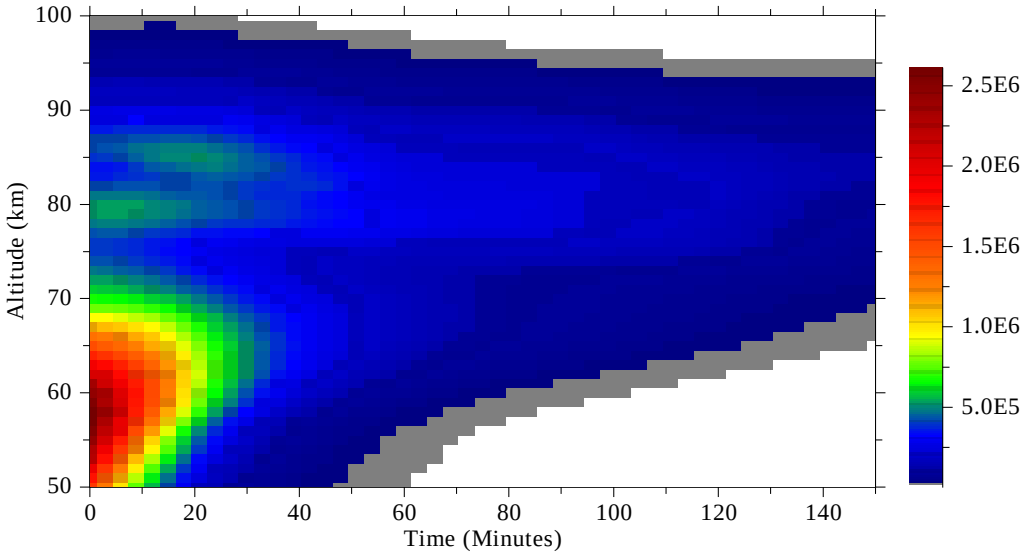

Figure 6.1: Singlet Delta decay as measured by IRIS around the equator. At time zero the sun is at 0° Solar Elevation Angle.

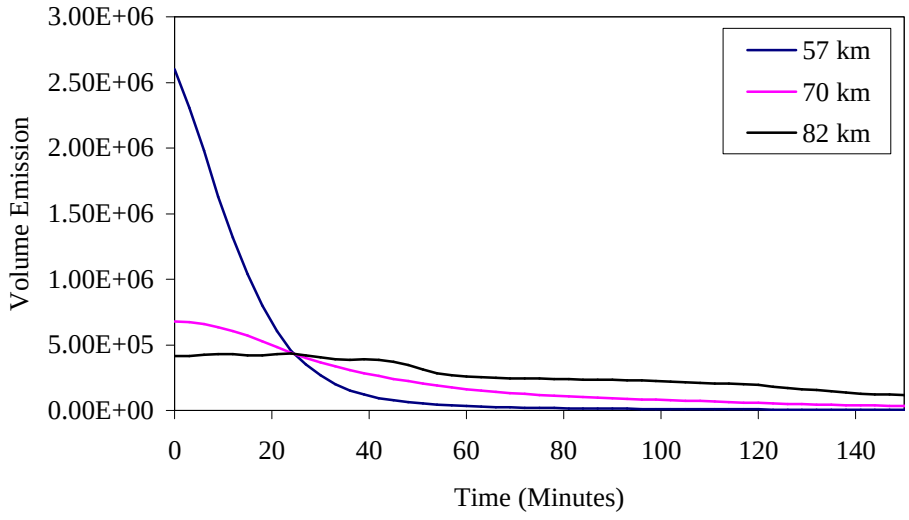

Figure 6.2: Singlet Delta decay at three different altitudes taken from the IRIS measurements in Figure 6.1

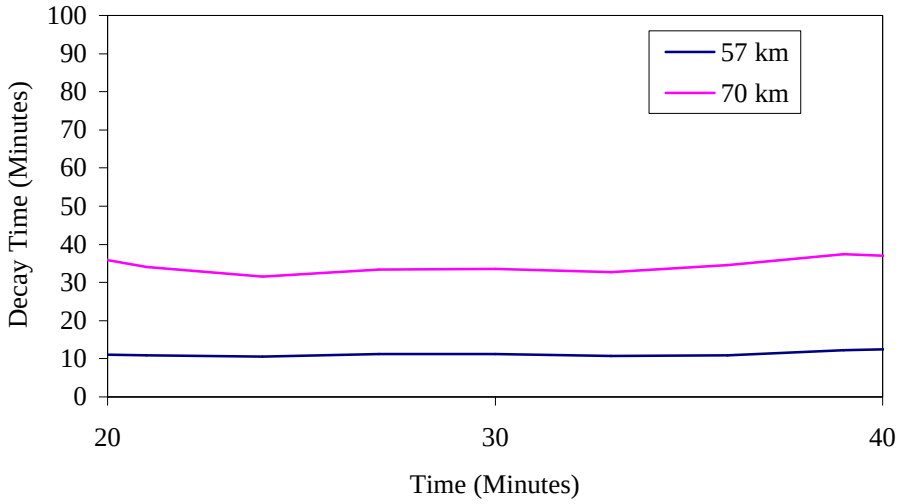

Figure 6.3: Singlet Delta decay for 57 and 70 km calculated from the IRIS measurements shown in Figure 6.2

below the horizon at 57 km (as measured by IRIS) is approximately 10 minutes and at 70 km approximately 35 minutes. It will be shown that similar decay times are obtained from TOP2000 measurements of the total column decay for the assumption that the singlet delta decay is heavily weighted to one altitude.

6.3 Measured Decay Times

The processed data from the TOP2000 measurements made in Eureka was analyzed to determine the scientific value of instrument. To verify its functionality the decay times of singlet delta were determined.

The processed data from Eureka, NU on March 9, 2004 were analyzed to determine the singlet delta emission decay times. The processed data for the narrow channel of TOP2000 along with the solar elevation angle (SEA) is plotted in Figure 6.4. At late twilight (SEA = -10 degrees) the signal to noise (S/N) ratio is 3. The

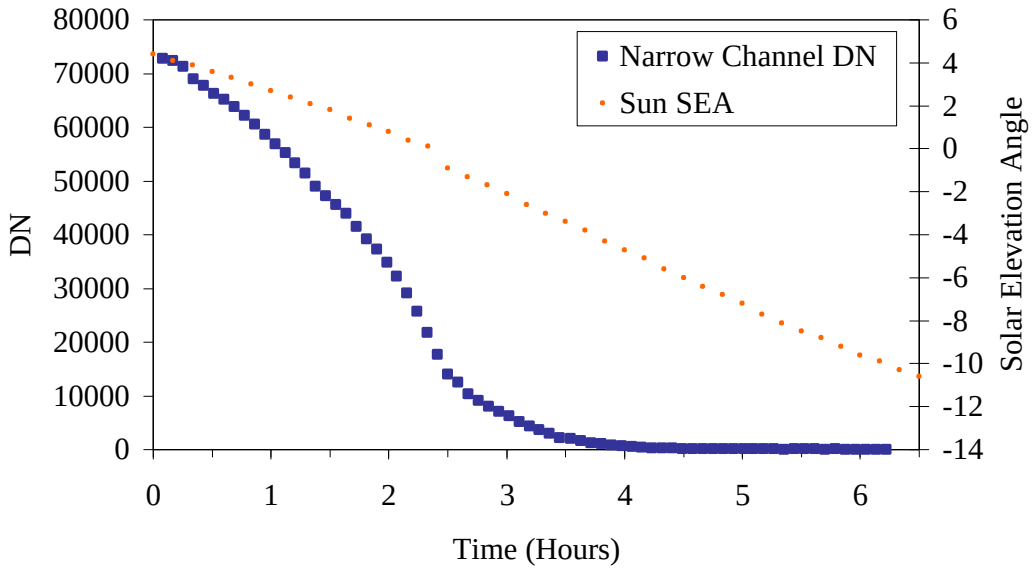

Figure 6.4: Processed narrow channel data and solar elevation angle (SEA) for Eureka, NU March 9, 2004

measured signal decay is the total column brightness of singlet delta measured at the ground. The altitude profiles of the singlet delta emission at each given time of the TOP2000 measurements in Figure 6.4 would be similar to those measured by IRIS and shown in Figure 6.1. While the sun is still above the horizon the narrow band signal is dominated by the 1.27 micron light scattered in the lower atmosphere. As the sun sets so the UV source for ozone photolysis, and production of singlet delta, begins to shut off at the lower altitudes from increased attenuation because of the longer path lengths through the atmosphere. Once the sun is far enough below the horizon the scattered light is also attenuated. The valid data for analysis of the singlet delta emission decay times is when the narrow channel is dominated by the singlet delta emission and there is no new production of singlet delta. At times when there is a scattered background component in the narrow band signal the two channel photometer method using the two equations to solve for both the emission and background must be used (this will not be done in this work).

The total column singlet delta emission brightness at a given time (t) measured by TOP2000 in the narrow channel can be described as

$$\mathrm{DN}_N(t) = k_N B_o(t) \int B_s(\lambda) F_N(\lambda) \mathrm{d}\lambda \tag{6.1}$$

where DN_N is the measured signal level in DN, k_N is the narrow channel calibration constant (as given in Table 4.1 for different gain settings), B_o is the singlet delta emission spectrum amplitude, B_s is the normalized singlet delta spectrum (as shown in Figure 2.1), F_N is the spectral response of the narrow channel (shown in Figure 4.9) and λ is a wavelength.

The following again uses the the assumptions made in Chapter 2 and demonstrated in the previous section that the total decay of singlet delta measured at the ground at a given time (t) is dominated by the emission at the lower altitudes around the time dependent peak seen in Figure 2.5. During the time when the narrow channel is measuring only the singlet delta emission then the measured DN of the narrow channel is proportional to the B_i, equation 2.21, which can be re-written as

$$\mathrm{DN}_N(t) = C \left[O_2^*\right]_o \ e^{-\lambda(t)t} \tag{6.2}$$

where C is a proportionality constant, $\left[O_2^*\right]_o$ is the initial concentration of singlet delta and λ is the total decay time constant at time t.

To solve for the total decay times, the natural log of equation 6.2 is taken giving

$$\ln\left(DN_N(t)\right) = -\lambda(t)t + \ln\left(DN_N(0)\right) \tag{6.3}$$

The total decay time constant at time t is the slope of the decay curve at time t of the $\ln\left(DN_N(t)\right)$ vs t plot. The natural log of the processed narrow channel DN for Eureka, NU on March 9, 2004 gives the plot shown in Figure 6.5. The time axis was started at 2.5 hours to zoom in on the twilight decay of the singlet delta measurements. A running average was used with this data to remove the small fluctuations of the natural log DN data that affect the calculations to determine the slopes. The total decay times $(1/\lambda)$ calculated from the slopes of the $\ln\left(DN_N(t)\right)$

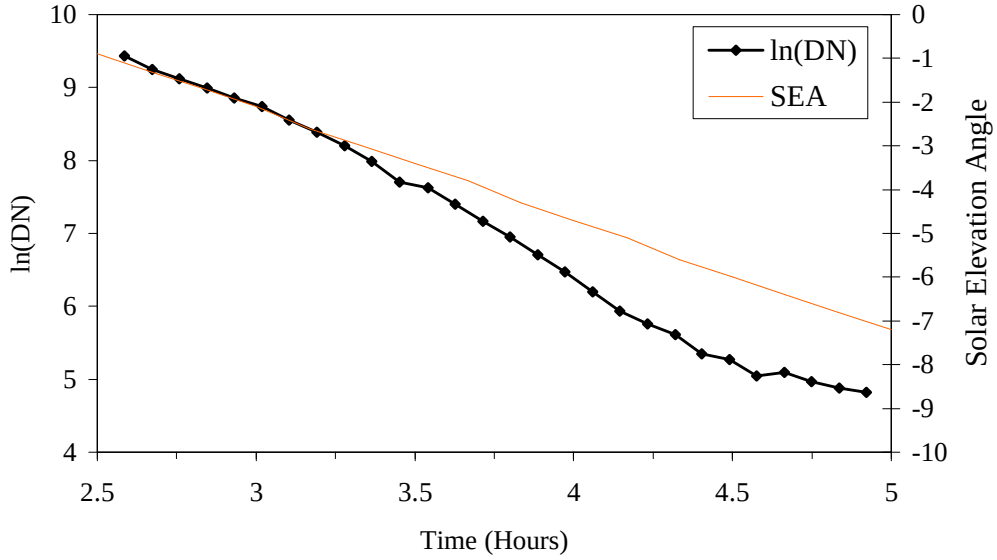

Figure 6.5: Natural log of the narrow channel data for Eureka, NU March 9, 2004

vs t plot shown in Figure 6.5 are plotted in Figure 6.6 along with the solar elevation angle (SEA).

The time when the background scattered light is a negligible component of the measured signal can be determined from the time when the narrow and wide channel ratio of the TOP2000 measurements becomes constant. When the background scattered light signal is negligible the wide channel of TOP2000 measures only the singlet delta emission (with less sensitivity then the narrow channel). The result of dividing the wide channel by the narrow channel measurements made by TOP2000 on March 9, 2004 is shown in Figure 6.7. The solar conditions at Eureka, NU were such that the background scattered light was not attenuated until well after production of singlet delta from the UV light had stopped. In Figure 6.7 the first constant ratio at approximately 1.4 is when both channels are dominated by the background scattered light. Between 3.5 and 4.5 hours the sun is setting and the scattered light is decreasing, this reduces the wide channel signal more then the narrow channel. From the ratio plot the background scattering is completely attenuated and only

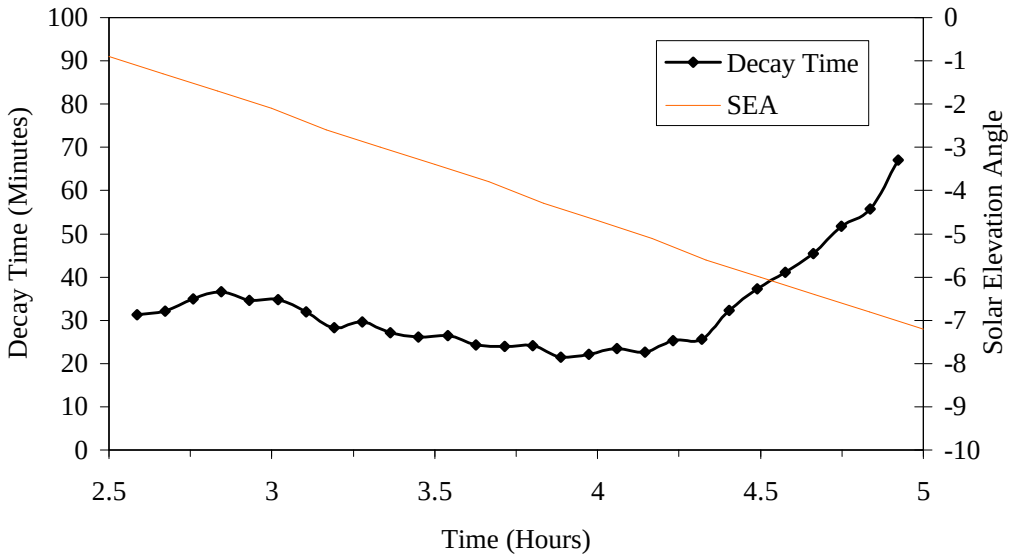

Figure 6.6: Calculated decay times for singlet delta from TOP2000 for Eureka, NU March 9, 2004

singlet delta emission remains at approximately 4.5 hours when the ratio is approximately constant. This occurs at a solar elevation angle of approximately -6 degrees. Therefore valid singlet delta emission decay times can be determined from the Eureka measurements on March 9, 2004 once the sun has passed 6 degrees below the horizon.

Once the sun has dropped below -6 degrees the light for production of ozone has been shut off for some time and the scattered light that reaches the atmosphere above the photometer is negligible. At this point the narrow channel signal is detecting the decaying singlet delta emission. In Figure 6.6 the shorter decay times correspond to the rapid decay of singlet delta at lower altitudes. As the altitude of the dominant decay increases the measured decay time increases to approximately 67 minutes which agrees with the measured 65 minute singlet delta radiative lifetime (1/A). As described in Chapter 2 this is the dominant decay time at higher altitudes.

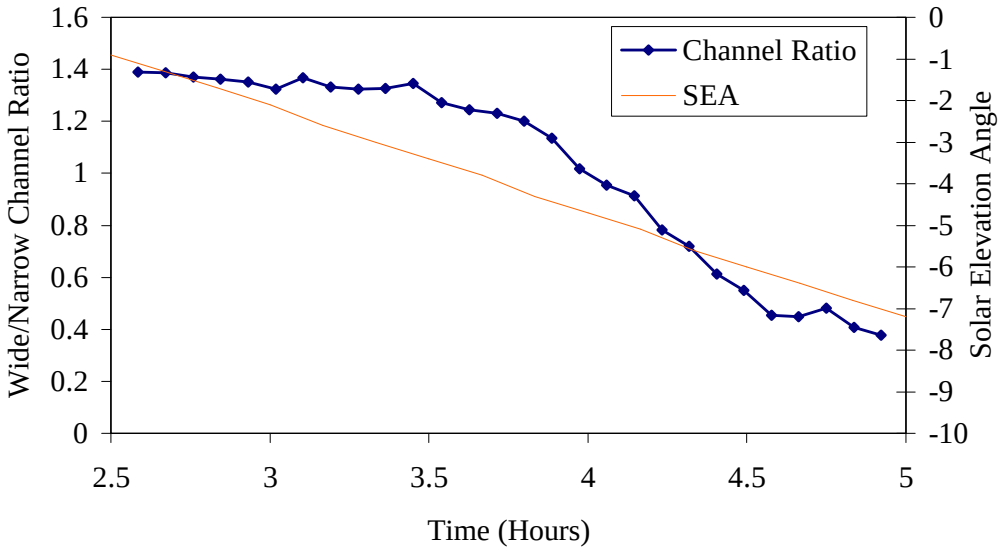

Figure 6.7: The wide and narrow channel ratios for Eureka, NU March 9, 2004 used to determine when the background scattered light is negligible in the vertical column above TOP2000.

6.4 Comparison of Data Measurements

Eureka provides a unique set of measurements as the sun sets slowly to low solar elevation angels compared with other locations of the world (i.e. away from the poles). Measurements were also made in Saskatoon and analyzed in the same way as the Eureka data to determine singlet delta decay times for comparison.

The calculated singlet delta decay times from the measurements made by TOP2000 from the roof of the Physics Building at the University of Saskatchewan on August 19, 2004 are shown in Figure 6.8. It is evident from Figure 6.8 that the sun sets very quickly (from 5 to 10 degrees below the horizon within half an hour) during this time of the year. In order to measure the lower altitude decay rates the shutter open and closed period was reduced compared to the Eureka shutter open and closed time. In this way less data were used in averaging for a single value and increased the noise in the later twilight data. The "dip" in the data point at approximately

1.8 hours in Figure 6.8 can be explained by this noise. Even though the singlet delta decay was not measured as late into the twilight as in Eureka the curve in Figure 6.8 still shows the expected increase in the decay time of singlet delta with time. As with the Eureka data while the sun is less than approximately 6 degrees below the horizon the detected singlet delta emission brightness in the narrow channel still contains scattered light. Valid decay time measurements only occur when the sun has dropped below -6 degrees. In Figure 6.8 this occurs between 1.6 and 1.7 hours (hours after data collection started) and the decay time increases from around 10 minutes to 44 minutes.

The calculated decay times for the Eureka data on March 9, 2004 and the Saskatoon data on August 19, 2004 are both plotted in Figure 6.9. At time zero the solar elevation angle for the Saskatoon and Eureka decay times is approximately -4.8 degrees. The difference in decay times between the Eureka measurements and the Saskatoon measurements can be explained by the difference in setting time of the sun. In Saskatoon the sun set quickly therefore the lower altitude singlet delta (with shorter lifetimes) had not fully decayed when the sun passed below -6 degrees solar elevation angle. In Eureka the sun set much slower than in Saskatoon and therefore by the time a solar elevation angle of -6 degrees was reached by the sun the lower altitude singlet delta had completely decayed. The decay time at time zero for the Eureka measurements therefore is longer than the Saskatoon decay time at time zero.

The other noticeable difference between the singlet delta decay curves from Eureka and Saskatoon shown in Figure 6.9 is the rate at which the decay times increase. The Saskatoon decay times increase faster then the Eureka decay times. This again is explained by the difference in solar conditions. In Eureka since the sun sets slower the higher altitude molecular oxygen was excited by the sun for a longer period as the sun was setting producing high altitude singlet delta longer. For the solar conditions in Saskatoon the sun set quickly so effectively shutting off all production and scattering of singlet delta at the same time. In other words in Eureka high

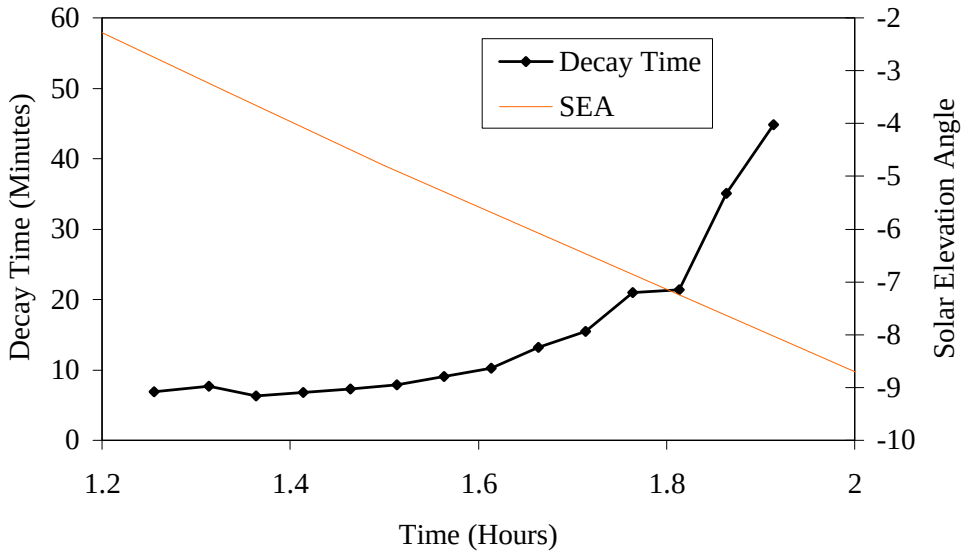

Figure 6.8: Calculated singlet delta decay times from TOP2000 measurements at Saskatoon, SK August 19, 2004.

altitude singlet delta was produced longer than in Saskatoon on the given days and therefore did not start decaying away without production until later in the twilight.

The slower setting sun in Eureka allowed for measurements by TOP2000 to extend later into the twilight. In order to capture enough samples during the early twilight in Saskatoon the shutter period was reduced. The reduced shutter open and closed time meant there were less data to average and so a decreased signal to noise ratio. During early twilight this effect was minimal since lower gain settings were used. However, during later twilight the effect was noticeable and limited analysis of the singlet delta emission measurements made in Saskatoon in late twilight. It is evident from the Saskatoon data collected in August of 2004 that the optimal operating settings of TOP2000 will need to be investigated for the different solar conditions throughout the year.

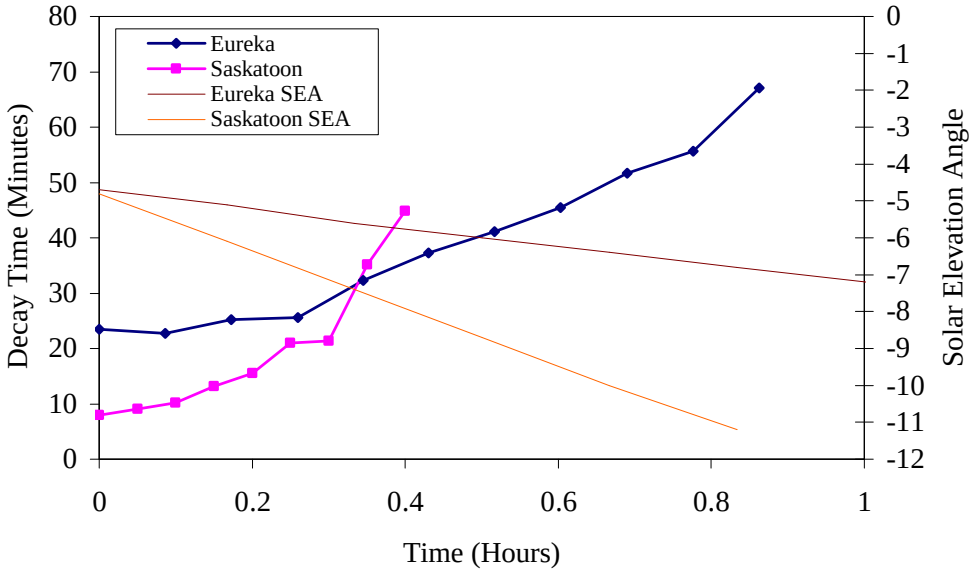

Figure 6.9: Comparison of decay time data between Eureka, NU (March 9, 2004) and Saskatoon, SK (August 19, 2004)

6.5 Conclusions

An example of the altitude profiles of singlet delta during the twilight decay as measured by the IRIS instrument was presented to validate the assumptions made in Chapter 2. Using these assumptions and the steps outlined the calculation of singlet delta decay rates for a given day of twilight data collected at Eureka in 2004 was presented. Singlet delta decay rates measured from Saskatoon in 2004 by TOP2000 were also given and compared to the Eureka decay times. From the analyzed data it is evident that the developed two channel photometer, TOP2000, is capable of making scientific measurements of singlet delta total column emission rates.

Chapter 7

Summary and Future Work

7.1 Summary of Presented Work

The history of singlet delta measurements was presented in Chapter 2. The early measurements of this atmospheric airglow provided valuable information about the chemical composition of the earths atmosphere. A technique to detect the singlet delta emission within a large background continuum using a two channel photometer was developed. The early two channel photometers were used on different platforms such as rockets and balloons as well as on the ground. The detection of singlet delta at the ground using a two channel photometer was given and some scientific experiments that can be conducted with the instrument were described.

Over the years that the two channel photometer has been used several designs have improved the functionality beyond the original proof of concept. However, all previous versions have used lead sulphide (PbS) detectors to convert the input light to an electrical signal. With the development of InGaAs photodiodes for optical communications an improved detection method was available and allowed another upgrade of the photometer. Chapter 3 outlines the design of TOP2000 that uses the InGaAs photodiodes, computer controlled lock-in amplifiers and microprocessor control. The computer that is interfaced serially to the instrument sends commands

that set the lock-in amplifier phase, offset and gain and controls the data collection from TOP2000. This computer control allows the instrument to operate without manual intervention by a user, which is important for operation in extreme cold weather conditions. To house the instrument during operation in the extreme cold an environmental box was built that included a thermostatically controlled strip heater, air circulation and insulation.

Once TOP2000 was completed and in working order several tests were conducted to characterize the instrument performance. First the proper lock-in amplifier phase settings were determined. The phase difference between the modulated input electrical signal from the pre-amplifiers and the reference input from the tuning fork chopper signal had to be minimized. With the phase settings determined tests to determine the dark output offset characteristics were performed. The increase in output offset with increase in lock-in amplifier gain setting was recorded. However, the major performance limitation of the instrument proved to be the temperature dependance of the output offset. The dark output offset was influenced by quite small changes in the ambient operating temperature, this affected the measurements made while operating in the environmental box in Eureka, NU in the fall of 2003. The major noise sources of the instrument were analyzed. An explanation for the temperature sensitivity of the dark output offset was attempted but not satisfactorily explained. Histograms of the output noise at different gain settings were given and provided information on the overall performance of the instrument (i.e. the required DN of signal in order to accurately separate it from the dark output offset).

Two calibrations were made for TOP2000 in the optics laboratory of the Physics Building at the University of Saskatchewan. The wavelength calibration was made with a scanning monochromator to generate approximately single wavelength output. The output wavelengths were scanned around the 1.27 micron region to determine both the wide and narrow channel spectral responses. The absolute calibration was made using a black body radiation source to generate a known brightness input to TOP2000. The black body source was operated at different set temperatures

and using Planck's function the brightness spectrum at each temperature from the output aperture was determined. The absolute calibration measurements were used to determine the absolute brightness calibration constants for both the narrow and wide channels, k_N and k_W respectively.

The evolution of measurements, the modifications required to improve the scientific value of the measurements and the steps for processing the useable data for further analysis were presented in Chapter 5. During operation of TOP2000 in Saskatoon the temperature sensitivity of the output offset was known and it was planned to use a look-up table with temperature and offset information to remove this effect. However, the data collected during operation of TOP2000 in the environmental box in Eureka, NU in the fall of 2003 proved that this method was inadequate. Modifications to the environmental box were made in an attempt to improve the temperature control and to add periodic dark output offset measurements. The PID temperature controller and the added extra heater did not improve the temperature ripple produced in the data. However, the shutter system provided intermittent dark offset data that could be subtracted from the shutter open data to remove the dark offset and its temperature dependent fluctuations. The steps required to process the data collected in Eureka, NU during the spring 2004 campaign were outlined.

In Chapter 6 the singlet delta altitude profiles during the twilight decay as measured around the equator by the IRIS instrument were presented. The altitude profiles are a sample of the structure in the total column brightness (sum of all altitudes at each time) as measured from the ground by TOP2000. By showing the decay of singlet delta at three different altitudes the assumption made in Chapter 2 that the singlet delta decay time at a given time could be assumed to be from a single altitude was validated. Using the steps outlined in Chapter 2 the singlet delta decay rates were calculated for a set of twilight measurements made in Eureka. The calculated decay times from the TOP2000 measurements agreed with the modelled decay times. The Eureka decay times were then compared with measurements made

from Saskatoon with TOP2000. The ability of TOP2000 to make scientifically valid measurements of the singlet delta emission was demonstrated in Chapter 6.

7.2 Recommendations for Future Work

Further modifications to the shutter system and the computer software have been made by a summer student working with the Infrared Research Group. These modifications will improve the operation of TOP2000 as a stand alone instrument by providing computer controlled shutter operation and automatic gain changes. TOP2000 as designed and developed for this research project can now be operated with minimal user intervention allowing long term ground based measurements of the singlet delta emission to be made. For completely independent operation (no requirements for a controlled environment such as a window hatch in a building) improvements must be made to the environmental box to cover operation in all weather conditions. Currently the box is designed to operate in cold weather and does not allow TOP2000 to be run during hot or rainy weather.

In a further attempt to understand the temperature sensitivity of TOP2000 the instrument was operated with several thermocouples measuring the temperatures at different points within the environmental box. The results of this experiment showed a potential temperature gradient within the environmental box that could help explain the complex temperature ripple in the dark output offset of TOP2000. Further testing of the temperature control within the environmental box and the temperature sensitivity of TOP2000 is required.

The used optical design was from the original two channel photometer design which employed large area detectors. The small diameter of the InGaAs photodiodes means that only a part of the focused spot is used. A properly matched optical system and photodiode detector would increase the minimum detectable signal level (improved signal to noise).

7.3 Conclusions

Once the instrument, TOP2000, was complete its output performance was characterized. The biggest issue found with the instrument performance was the fluctuations of the output offset for even small changes in ambient temperature. Improvements made to the environmental housing allowed the removal of the temperature effects so that TOP2000 was able to collect data of scientific value. This was demonstrated with an analysis that showed the expected increase of the total decay times towards the radiative lifetime of singlet delta as evening twilight progressed.

The original project objectives were accomplished. A two channel photometer was designed with updated technology from the earlier versions. Minimal user intervention is required for the operation of the photometer. During two separate campaigns the two channel photometer was successfully operated in the high arctic.

A list of recommendations are only for improvements to the existing system. TOP2000 is currently a working instrument that has demonstrated the ability to collect scientifically relevant data. This data can now be used to determine singlet delta and ozone total column and vertical height profile concentrations. If it is operated for an extended period at a given location the collected data can help determine trends in singlet delta and ozone concentrations. The scientific data can also be used to help verify and validate measurements made with the infrared imager system (IRIS) on board the Odin satellite.

Appendix A

For molecular oxygen $a^1\Delta_g - X^3\Sigma_g^-$ represents an energy transition from the excited state energy level ($a^1\Delta_g$) to the ground state energy level ($X^3\Sigma_g^-$); this is illustrated in Figure A.1. For the infrared atmospheric emission from the singlet delta ($a^1\Delta_g$) energy level there are two possible wavelengths of light (1.57 and 1.27 microns). The 1.27 μm emission can be described as the 0,0 ($a^1\Delta_g - X^3\Sigma_g^-$), where 0,0 represents the vibrational levels of the excited singlet delta and the ground state. The 1.57 μm emission can be described as the 0,1 ($a^1\Delta_g - X^3\Sigma_g^-$) emission and the 1 represents the first vibrational level of the ground state $X^3\Sigma_g^-$.

Each energy level shown in Figure A.1 is described by standard spectroscopic notation. In this way the electron spin, electron angular momentum, total angular momentum and symmetry of the molecule in each state is defined.

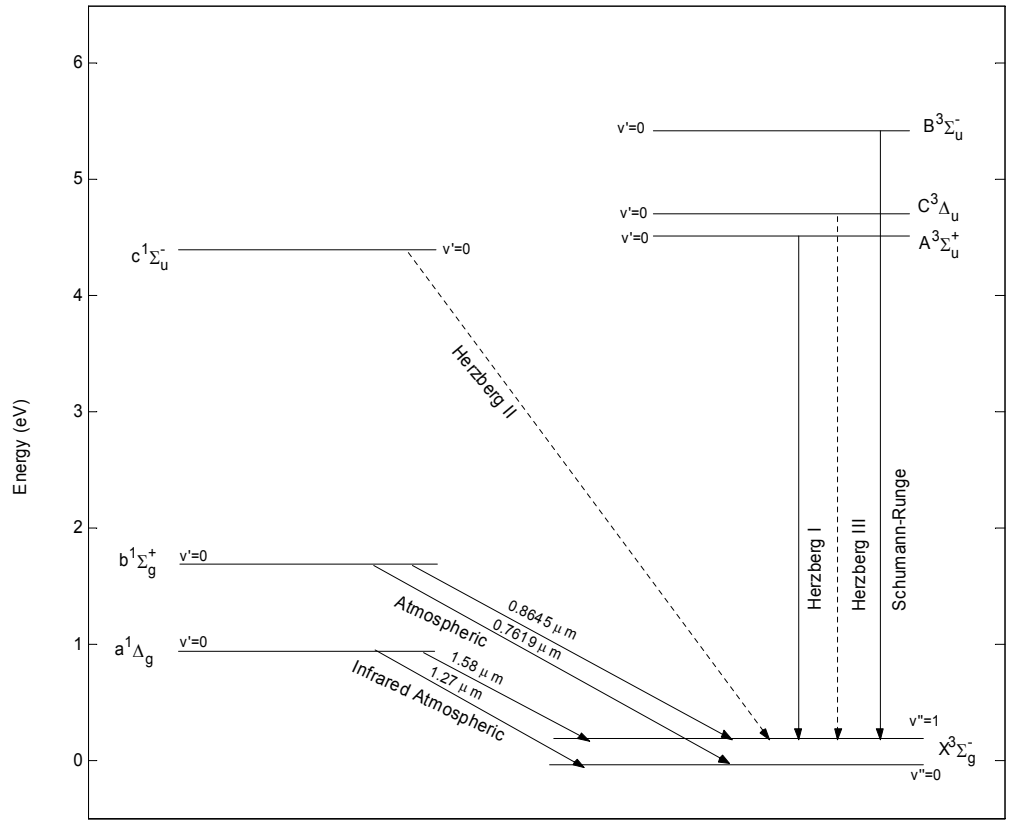

Figure A.1: Molecular Oxygen energy transitions.

References

[1] Herzberg, G.: "Photography of the Infra-Red Solar Spectrum to Wavelength 12,900 Å", Nature, vol. 133, p. 759, 1934.

[2] Vallance Jones, A., and A.W. Harrison: "$^1\Delta_g - ^3\Sigma_g$ O_2 Infrared Emission Band in the Twilight Airglow Spectrum", J. Atmos. Terr. Phys., vol. 13, p. 45, 1958.

[3] Noxon, J.F., and A. Vallance Jones: "Observation of (0,0) Band of the ($^1\Delta_g - ^3\Sigma_g$) System of Oxygen in the Day and Twilight Airglow", Nature, vol. 196, p. 157, 1962.

[4] Vallance Jones, A., and R.L. Gattinger: "The Seasonal Variation and Excitation Mechanism of the 1.58 μ $^1\Delta_g - ^3\Sigma_g$ Twilight Airglow Band", Planet. Space Sci., vol. 11, p. 961, 1963.

[5] Gattinger, R.L., and A. Vallance Jones: "The $^1\Delta_g - ^3\Sigma_g$ Bands in the Twilight and Day Airglow", Planet. Space Sci., vol. 14, p. 1, 1966.

[6] Noxon, J.F.: "Oxygen Spectra in Dayglow Twilight and During an Eclipse", Nature, vol. 213, p. 350, 1967.

[7] Evans, W.F.J., E.J. Llewellyn, and A. Vallance Jones: "Balloon-borne Observations of the Brightness Variations in the (0,0) Band of the ($^1\Delta_g - ^3\Sigma_g$) System of Oxygen in the Day and Twilight Airglow", Nature, vol. 213, p. 352, 1967.

[8] Evans, W.F.J., D.M. Hunten, E.J. Llewellyn, and A. Vallance Jones: "Altitude Profile of the Infrared Atmospheric System of Oxygen in the Dayglow", J. Geophys. Res., vol. 73, p. 2885, 1968.

[9] Haslett, J.C., and L.R. Megill: "Rocket Measurements of $O_2(^1\Delta_g)$", Can. J. Phys., 47, p. 2351, 1969.

[10] Wood, H.C.: "The Measurement and Interpretation of $O_2(a^1\Delta_g)$ Concentrations in the Atmosphere" Ph.D. Thesis, University of Saskatchewan, 1972.

[11] Lowe, R.P.: "Interferometric Spectra of Earths Airglow (1.2-MUM to 1.6-MUM)", Phil. Trans. Roy. Soc. London, Series A, vol. 264, p. 163, 1969.

[12] Evans, W.F.J., H.C. Wood, and E.J. Llewellyn: "Transmission of the 1.27μ Band Through the Atmosphere", Can. J. Phys., vol. 48, p. 5, 1970a.

[13] Evans, W.F.J., H.C. Wood, and E.J. Llewellyn: "Ground-based Photometric Observations of the 1.27μ Band of O_2 in the Twilight Airglow", Planet. Space Sci., vol. 18, p. 1065, 1970b.

[14] Evans, W.F.J., and E.J. Llewellyn: "Altitude Distribution of the $O_2(a^1\Delta_g)$ Nightglow Emission", J. Geophys. Res., vol. 77, p. 4899, 1972.

[15] Plemel, R.: "Ground Based Observations of $O_2(a^1\Delta_g)$in the Evening Twilight and During a Solar Eclipse" M.Sc. Thesis, University of Saskatchewan, 1974.

[16] How, P.J.: "Mesospheric Ozone Observations at C.F.S. Alert, N.W.T." M.Sc. Thesis, University of Saskatchewan, 1993.

[17] Thomas, R.J., C.A. Barth, D.W. Rusch, and R.W. Sanders: "Solar Mesosphere Explorer Near-Infrared Spectrometer: Measurements of 1.27-μm Radiances and the Interference of Mesospheric Ozone", J. Geophys. Res., vol. 89, p. 9569, 1984.

[18] Barth, C.A., D.W. Rusch, R.J. Thomas, G.H. Mount, G.J. Rottman, G.E. Thomas, R.W. Sanders, and G.M. Lawrence: "Solar Mesospheric Explorer: Scientific Objectives and Results", Geophys. Res. Letters, vol. 10, p. 237, 1983.

[19] Degenstein, D.A., E.J. Llewellyn, and N.D. Lloyd: "Volume emission rate tomography from a satellite platform", Applied Optics, vol. 42, no. 8, p. 1441, 2003.

[20] Llewellyn, E.J., N.D. Lloyd, D.A. Degenstein, R.L. Gattinger, S.V. Petelina, A.E. Bourassa, J.T. Wiensz, E.V. Ivanov, I.C. McDade, B.H. Solheim, J.C. McConnell, C.S. Haley, C. von Savigny, C.E. Sioris, C.A. McLinden, E. Griffioen, J. Kaminski, W.F.J. Evans, E. Puckrin, K. Strong, V. Wehrle, R.H. Hum, D.J.W. Kendall, J. Matsushita, D.P. Murtagh, S. Brohede, J. Stegman, G. Witt, G. Barnes, W.F. Payne, L. Pich, K. Smith, G. Warshaw, D.-L. Deslauniers, P. Marchand, E.H. Richardson, R.A. King, I. Wevers, W. McCreath, E. Kyrl, L. Oikarinen, G.W. Leppelmeier, H. Auvinen, G. Mgie, A. Hauchecorne, F. Lefvre, J. de La Ne, P. Ricaud, U. Frisk, F. Sjoberg, F. von Schele, and L. Nordh: "The OSIRIS Instrument on the Odin Spacecraft.", Can. J. Phys, vol. 82, p. 411, 2004.

[21] Mlynczak, M.G., S. Solomon, and D.S. Zaras: "An Updated Model for $O_2(a^1\Delta_g)$ Concentrations in the Mesosphere and Lower Thermosphere and Implications for Remote Sensing of Ozone at 1.27 μm", J. Geophys. Res., vol. 98, p. 18639, 1993.

[22] Sica, R. J.: "Inferring Middle-Atmospheric Ozone Height Profiles From Ground Based Measurements of Molecular Oxygen Emission Rates", Can. J. Phys., vol. 69, p. 1069, 1991.

[23] Evans, W.F.J.: "An Investigation of the Temporal and Spatial Variations of the Infrared Atmospheric Bands of Molecular Oxygen in the Airglow" Ph.D. Thesis, University of Saskatchewan, 1967.

[24] Kasap, S.O.: Optoelectronics and Photonics. Prentice Hall, 2001.

[25] Meade, M.L.: Lock-in amplifiers: principles and applications. Peter Peregrinus Ltd., 1983.